THE ASTROPHYSICAL JOURNAL, Vol. 159, February 1970

ROTATION OF THE ANDROMEDA NEBULA FROM A SPECTROSCOPIC SURVEY OF EMISSION REGIONS*

VERA C. RUBIN† AND W. KENT FORD, JR.†
Department of Terrestrial Magnetism, Carnegie Institution of Washington and
Lowell Observatory, and Kitt Peak National Observatory‡
Received 1969 July 7; revised 1969 August 21

ABSTRACT

Spectra of sixty-seven H II regions from 3 to 24 kpc from the nucleus of M31 have been obtained with the DTM image-tube spectrograph at a dispersion of 135 Å mm^{-1}. Radial velocities, principally from Hα, have been determined with an accuracy of ±10 km sec^{-1} for most regions. Rotational velocities have been calculated under the assumption of circular motions only.

For the region interior to 3 kpc where no emission regions have been identified, a narrow [N II] λ6583 emission line is observed. Velocities from this line indicate a rapid rotation in the nucleus, rising to a maximum circular velocity of $V = 225$ km sec^{-1} at $R = 400$ pc, and falling to a deep minimum near $R = 2$ kpc.

From the rotation curve for $R \leq 24$ kpc, the following disk model of M31 results. There is a dense, rapidly rotating nucleus of mass $M = (6 \pm 1) \times 10^9 M\odot$. Near $R = 2$ kpc, the density is very low and the rotational motions are very small. In the region from 500 to 1.4 kpc (most notably on the southeast minor axis), gas is observed leaving the nucleus. Beyond $R = 4$ kpc the total mass of the galaxy increases approximately linearly to $R = 14$ kpc, and more slowly thereafter. The total mass to $R = 24$ kpc is $M = (1.85 \pm 0.1) \times 10^{11} M\odot$; one-half of it is located in the disk interior to $R = 9$ kpc. In many respects this model resembles the model of the disk of our Galaxy. Outside the nuclear region, there is no evidence for noncircular motions.

The optical velocities, $R > 3$ kpc, agree with the 21-cm observations, although the maximum rotational velocity, $V = 270 \pm 10$ km sec^{-1}, is slightly higher than that obtained from 21-cm observations.

I. INTRODUCTION

The Andromeda Nebula offers a unique opportunity for the study of the dynamics of a galaxy. Because of its large angular extent on the sky, it is possible to observe individual emission regions spectroscopically and, in principle, to map the velocity field of a galaxy which resembles our Galaxy. In practice, however, the extreme faintness of the regions makes detailed optical studies very time-consuming, if not impossible. The very early observations of M31 were restricted to the bright central regions. In 1914, from observations made with the Lowell Observatory 24-inch refractor, V. M. Slipher (1914) reported inclined absorption lines across the nucleus of M31. From absorption lines, Pease (1918) measured the rotation out to 150 seconds of arc from the nucleus on a single plate of 79 hours' exposure, taken in 1917 during the months of August, September, and October. The Mount Wilson 60-inch reflector was used, the dispersion[1] was 192 Å mm^{-1}, and the resulting values are of sufficiently high accuracy to warrant serious scientific consideration today.

The first large-scale study of motions in M31 was made by Babcock (1939) with the 36-inch Crossley telescope at Lick Observatory. His observations included spectra of the unresolved central nucleus (exposure times 25 minutes to 22 hours) and a few spectra of

* *Contributions from the Kitt Peak National Observatory*, No. 492.

† Visiting Astronomer 1966, 1967, 1968, Lowell Observatory; and Visiting Astronomer 1967, 1968, Kitt Peak National Observatory.

‡ Operated by the Association of Universities for Research in Astronomy, Inc., under contract with the National Science Foundation.

[1] Drs. N. U. Mayall and R. Minkowski have pointed out that there is a misprint in Pease's paper, and the observed wavelength range is actually 3930–4950 Å, not 4930–4950 Å as published.

individual emission nebulosities (exposure times 7–22 hours). Velocities were determined from absorption lines in the central nucleus and from emission lines in the nebulosities. For many years, his results were the starting point for studies of the dynamics of M31. To date, the most extensive study of velocities in M31 is due to Mayall (1951; Baade and Mayall 1951), who obtained spectra of numerous fainter emission regions in M31 with the Crossley telescope; exposures often required two nights.

In the last 20 years, no additional optical velocities for emission regions in M31 have been added to the literature. During this time, however, velocity studies of M31 have been made from observations of the 21-cm line of H I. In addition, 688 individual emission regions in M31 have been identified by their Hα radiation by Baade (Baade and Arp 1964). Even more important, the use of image intensifiers has made it possible to reduce observing times by a factor of 10, making it possible to complete fairly ambitious observing programs in a few observing seasons. For all of these reasons, we have undertaken an observing program to obtain spectra of emission regions in M31. Our aims were threefold: (1) to observe the velocity field and determine the mass; (2) to study the variation of line-intensity ratios from region to region as a function of distance from the nucleus; and (3) to relate the velocities and line strengths to the spiral structure of M31. The present paper is concerned principally with the velocities and mass determination.

II. OBSERVATIONS OF THE EMISSION REGIONS

Using the 100-inch Mount Wilson telescope, Baade carried out an extensive survey to identify H II regions in M31 by their Hα radiation. Baade provided marked charts for Mayall and Kron; copies of these were kindly made available to us by Dr. Kron. From this material, we have observed sixty-seven emission regions distributed over all quadrants of M31, generally near the major axis. Baade found no H II regions less than 16′ (3.2 kpc) from the nucleus; the most distant region is at $R = 120'$ (24 kpc). We have attempted to observe all of the innermost and all of the outermost regions identified by Baade. A distance of $D = 690$ kpc is adopted for M31. At this distance $1' = 200$ pc. In M31, a typical Strömgren sphere will appear several seconds of arc in diameter. In Figure 1 (Plate 1), the locations of the emission regions observed spectrographically are shown superimposed on a photograph of M31.

The DTM image-tube spectrograph was used on the 72-inch telescope of the Ohio State and Ohio Wesleyan Universities at Lowell Observatory; spectra were also obtained with the same spectrograph, particularly in the nuclear region, on the Kitt Peak 84-inch telescope. The spectrograph incorporates a two-stage magnetically focused RCA cascaded image tube at the focus of a Cassegrain semisolid Schmidt camera designed by Dr. I. S. Bowen. Baked IIa-O plates were used to photograph the final P11 phosphor screen of the image tube. The spectrograms extend from Hβ through Hα in first order at a dispersion of 135 Å mm^{-1}, equivalent to 6.2 km sec^{-1} μ^{-1} at Hα. For the Perkins telescope, the scale perpendicular to the dispersion is 40″ mm^{-1}. The slit width is generally 1″.4 on the sky, which corresponds to 30 μ on the plate. Magnitudes of the emission regions have been estimated by Baade to range from 16 to 21. None of these was visible in the telescope; hence, offsetting and guiding from nearby stars was necessary. Typical exposure times were 60–90 minutes. Whenever possible, the spectrograph was rotated so that spectra of two emission regions could be recorded simultaneously. During each exposure, a second plate was exposed on a photometric step wedge to provide a density calibration. Slit-curvature plates were also obtained so that the measured velocities could be corrected for the distortion of the optical image-tube system. All plates were measured on a Mann two-coordinate measuring machine, and conventional procedures were used to make reductions with an IBM computer.

The original aim of the observing program was to obtain two plates from different observing sessions for each emission region. This aim has not been completely achieved.

For forty-six of the sixty-seven regions we have two or three spectra each. For the remaining twenty-one regions we have only one plate each; however, seventeen of these twenty-one plates have been judged good or excellent, so the accuracy of the total study would have been only slightly increased by obtaining more spectra of these same regions. The total number of measured spectra is 123. In Table A1 in the Appendix a detailed record of observations is given.

We list in Table 1 a summary of the observations and reductions. Successive columns give the Arp number of the region, the nebular coordinates on the plane of the sky, X directed along the major axis and positive with increasing right ascension, Y directed along the minor axis and positive to the south. Values of X and Y are taken from Baade and Arp (1964). Often a plate contains both the spectrum from the Arp region and emission from a weaker uncataloged region. A few of these were measurable, and the region is identified in Table 1 by an "a" following the Arp number of the nearby brighter region. Columns (4) and (5) list the coordinates R and θ in the plane of M31 for each region.

The mean observed velocity of each region is tabulated in column (6). For a well-exposed plate, lines of Hβ; [O III] $\lambda\lambda$4959, 5007; He I λ5876; [O I] λ6300; [N II] λ6548; Hα; [N II] λ6583; and [S II] $\lambda\lambda$6717, 6731 are observed. In Figure 2 (Plate 2), we reproduce spectra of some of these regions. For the weakest regions, only Hα is seen. Generally, [O III] λ5007, Hα, and [N II] λ6583 are measured for velocity; Hα is always given double weight in forming the mean velocity for a single plate. The mean velocity from a single plate is assigned a weight depending on the quality of the plate: good or excellent, weight = 1; fair, weight = 0.75; poor, weight = 0.5. When several spectra have been measured for a single region, a weighted mean observed velocity is formed. In column (7) we list for each region the sum of the weights from all plates of the region. For the outermost region, $R = 120'$, we observe only [O III] $\lambda\lambda$4959 and 5007, but no Hα. Therefore, its velocity is less certain than the others.

For forty-three regions with more than one measured velocity and a value of 1.5 or greater for the sum of the weights, the average deviation from the mean is 10 km sec^{-1}. Therefore, an average error ϵ of the mean observed velocity has been assigned as follows: with a value for the sum of the weights of 1.5, ϵ = 10 km sec^{-1}; with a value of 1, ϵ = 15 km sec^{-1}; with a value of 0.5, ϵ = 25 km sec^{-1}.

The only earlier measures with which we can compare these velocities are from Mayall (1951). Mayall observed twenty-seven emission regions near the major axis; we have observed seventeen of these regions. The velocity agreement is not good. For ten regions near the NE major axis, the average difference ΔV (our value less Mayall's) is -97 km sec^{-1}; for seven regions near the SW major axis, $\Delta V = -31$ km sec^{-1}. However, Mayall (private communication) has cautioned against putting too much weight on his velocities, because of his long exposures and low dispersions. We have therefore not made use of these early values.

Deharveng and Pellet (1969) have recently obtained interferograms of the NE arm ($R \sim 50'$) of M31, and have obtained velocities by using Hα at a dispersion of 26 Å mm^{-1}. We have velocities for eight emission regions located within their fields; for six of these regions they have observations nearby (within 15″). In no case, however, have we both observed the identical region. Our observations refer to emission from starlike condensations, while the Hα emission they observe comes from the diffuse surrounding regions. The velocity agreement is excellent, however. For Arp 95 and 97, we observe a mean velocity $\langle V \rangle = -185 \pm 14$ km sec^{-1}; Deharveng and Pellet observe two adjacent regions (b339017, b339018) with $\langle V \rangle = -184 \pm 12$ km sec^{-1}. For the H II complex Arp 162, 162a, 165, 167, we observe $\langle V \rangle = -134 \pm 13$ km sec^{-1}; two adjacent regions from DP (e247005, e247006) have $\langle V \rangle = -124 \pm 8$ km sec^{-1}. The listed errors are external mean errors.

TABLE 1

POSITIONS AND VELOCITIES OF EMISSION REGIONS IN M31

Arp No. (1)	X (2)	Y (3)	R (4)	θ (5)	V_{obs} (km sec^{-1}) (6)	Weight (7)	V_{rot} (km sec^{-1}) (8)	OB Association (9)
55	+ 14.8	+ 1.5	16.2	24.5	−241	1.8	66±11*	Outside 2
23	+ 6.9	+ 5.0	23.0	72.6	−219	1	278±52	1
24	+ 7.1	+ 5.2	24.0	72.7	−228	1	250±52	1
74	+ 16.5	+ 4.2	24.7	48.3	−123	1	273±23	2
75	+ 16.5	+ 4.3	25.2	49.3	−116	1	290±24	2
162	+ 33.6	+ 8.8	51.4	49.1	−149	1	237±24	48
162a	+ 33.6	+ 8.8	51.4	49.1	−146	1	242±24	48
165	+ 33.8	+ 8.8	51.6	49.2	−143	1	247±24	48
204	+ 49.7	+ 3.6	52.1	17.8	− 45	2	275±11	50
204a	+ 49.7	+ 3.6	52.1	17.8	− 37	1	284±16	50
210	+ 51.7	+ 1.7	52.2	8.4	− 40	1.8	270±10	51
212	+ 51.8	+ 1.9	52.5	9.4	− 46	1	264±16	51
167	+ 34.1	+ 9.0	52.5	49.5	− 97	1	321±24	48
95	+ 20.1	+11.2	53.7	68.0	−176	0.5	341±68	39
97	+ 20.3	+11.3	54.1	67.9	−187	2	309±27	39
185	+ 41.2	+ 8.8	56.8	43.6	−106	1	275±21	95
184	+ 41.0	+ 8.9	56.9	43.9	−137	2	232±14	95
216	+ 52.7	+ 8.3	64.3	35.0	− 77	1.8	280±12	97
217	+ 52.7	+ 8.4	64.6	35.0	− 59	0.5	303±31	97
236	+ 64.0	+ 9.1	75.7	32.2	−129	2	208±12	150
249	+ 92.9	+ 2.4	93.4	6.6	− 92	2	215±10	...
250	+ 98.2	+ 4.9	100.5	12.4	−112	2.2	198±10	...
521	+ 8.7	− 4.6	22.1	293°	−208	1	240±39	...
521a	+ 8.7	− 4.6	22.1	293°	−263	1	96±39	...
519	+ 7.7	− 4.8	22.6	290°	−157	2	433±30	14
600	+ 41.3	− 5.3	47.4	330°	− 90	1	248±18	54
599	+ 41.2	− 5.3	47.5	330°	− 59	0.5	285±29	54
616	+ 46.2	− 4.6	50.4	336°	− 62	2	267±11	53
577	+ 34.9	− 8.9	52.8	311°	−129	1	265±23	110
565	+ 26.6	−13.2	64.3	294°	−163	2	340±25	...
628	+ 51.4	− 9.6	66.8	320°	−134	1.8	221±13	113
666	+ 70.0	− 0.4	69.9	359°	− 49	3	258±10	102
671	+ 70.2	− 0.6	70.2	358°	− 34	3	273±10	102
595	+ 40.8	−15.3	79.4	301°	−188	3	224±20	167
683	+ 76.6	−11.1	91.0	327°	−134	2.8	202±12	159
686	+ 85.9	− 7.0	91.3	340°	− 95	2	224±11	157
685	+ 84.5	− 8.3	92.2	336°	−116	1.8	206±11	157
688	+116.8	− 6.3	120.1	346°	− 47	2.8	267±10	...
275	− 15.2	+ 6.4	32.2	118°	−446	1.5	318±22	...
289	− 28.5	+ 4.3	34.2	146°	−519	1.5	270±12	22
303	− 38.3	+ 0.9	38.5	174°	−508	1.8	215±10	...
312	− 42.8	+ 1.4	43.2	172°	−567	2	277±10	78
284	− 23.2	+10.7	52.8	116°	−393	2	218±23	outside 86
290	− 28.6	+10.3	53.9	122°	−389	1.5	172±19	outside 84
297	− 33.0	+ 9.9	54.9	127°	−455	3	265±17	76
320	− 44.7	+ 7.7	56.2	143°	−492	1.5	248±13	82
338	− 56.8	+ 1.0	57.0	176°	−531	1.8	238±10	...
343	− 58.0	+ 4.2	60.9	162°	−547	1.5	266±11	134
330	− 47.6	+10.2	65.5	136°	−499	1	282±21	82
379	− 66.6	+ 2.2	67.3	172°	−543	2	252±10	136
359	− 64.4	+ 6.8	71.0	155°	−546	2	278±11	139
360	− 64.6	+ 6.9	71.5	154°	−523	2	253±11	139
352	− 62.7	+ 8.6	73.3	149°	−493	1	232±18	140
380	− 94.7	+13.3	111.6	148°	−475	2	212±12	186
415	− 14.0	− 2.8	18.6	221°	−389	1	121±20	20
415a	− 14.0	− 2.8	18.6	221°	−436	0.5	185±34	20
416	− 15.2	− 4.6	25.4	233°	−461	1	276±26	...
423	− 17.3	− 4.2	25.5	227°	−446	2	221±15	19
464	− 41.2	− 0.8	41.3	185°	−540	2.2	247±10	78
429	− 21.4	− 8.0	41.5	239°	−431	1	262±30	69
484	− 63.6	− 2.2	64.4	189°	−526	2.8	235±10	128
479	− 55.4	− 8.4	66.8	214°	−481	2	224±12	127
478	− 55.3	− 8.5	67.0	214°	−506	3	256±12	127
500	− 95.8	− 0.8	95.9	182°	−498	2	203±10	184
494	− 78.5	−14.9	102.7	220°	−510	2	282±13	182
493	− 78.4	−15.0	102.9	220°	−459	2	214±13	182
502	−113.6	− 0.5	113.6	181°	−513	2	219±10	...

* Average error of observed radial velocity, increased by projection factor $p = (R/X)$ csc 77°.

III. THE ROTATIONAL VELOCITIES, $R > 16'$ (3.2 KPC)

For an emission region with nebular coordinates R, θ, the observed radial velocity is related to the circular-velocity component $V(R)$ and the expansion component $E(R)$ through the equation

$$V_{\rm obs} - V_c = V(R) \sin \xi \cos \theta + E(R) \sin \xi \sin \theta , \quad (1)$$

where V_c is the systemic velocity of the galaxy. In terms of the observed coordinates X, Y, $\cos \theta = X/R$, $\sin \theta = (Y \sec \xi)/R$, $R = (X^2 + Y^2 \sec^2 \xi)^{1/2}$. The angle ξ is the angle between the line of sight and the perpendicular to the plane of the galaxy. For M31, a value of 77° for ξ is adopted because it is the mean of several optical determinations, and also because it was used by Burke, Turner, and Tuve (1964) and by Roberts (1966) and hence allows a direct comparison of the optical results with the 21-cm observations. A more detailed discussion of the geometrical parameters for M31 can be found

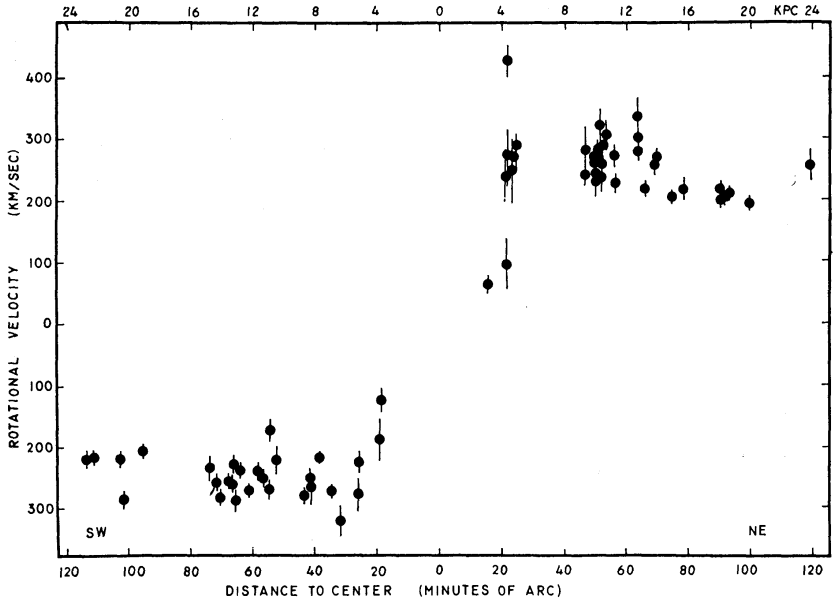

FIG. 3.—Rotational velocities for sixty-seven emission regions in M31, as a function of distance from the center. Error bars indicate average error of rotational velocities.

elsewhere (Rubin and D'Odorico 1969). The position angle of the major axis is taken as 38°. From symmetry considerations, and because it is near the mean value $V_c = -302$ observed from the [N II] λ6583 emission line at the nucleus, V_c is taken as -300 km sec^{-1}. The remaining assumption in equation (1) is that all motions are constrained to the principal plane of M31. If expansion motions are not present, $E(R) = 0$, and the second term in equation (1) vanishes. Hence, we can determine a circular velocity from the observed radial velocity of each emission region from the relation

$$V_{\rm obs} + 300 = V(R) \sin 77°(X/R) . \quad (2)$$

The calculated circular velocities are listed in column (8) of Table 1, along with the error of the circular velocities. Errors have been formed from the average errors of the radial velocities, increased by the projection factor $p = \csc 77° \sec \theta$. For regions along the major axis, $p = 1.026$; for regions with $\theta = 45°$, $p = 1.45$. In Figure 3 the circular velocities for all sixty-seven emission regions are plotted as a function of distance from the center. The velocities increase rapidly in the region $3.2 < R < 5.0$ kpc, and decrease slowly in the outer regions of the galaxy.

Many of the brighter emission regions in M31 are large, complex associations of emission regions and OB stars. However, there are also completely isolated Strömgren spheres. In an effort to obtain spectra from all parts of M31, we have generally observed no more than two regions within a single association, and have observed some of the isolated regions. In Table 1, column (9), we have classified the observed regions according to their membership in the M31 OB associations as defined by van den Bergh (1964). Fourteen of the regions we have observed are not in OB associations; the remaining fifty-three regions are distributed in thirty-four associations. Seventeen associations have velocities from two or more regions; for all association members the average deviation from the mean association velocity is 10 km sec^{-1}, or just equal to the average internal error in the radial velocity of an emission region. We conclude that the line-of-sight component of the velocity dispersion within an association is less than ± 10 km sec^{-1}, or less than 15 km sec^{-1} projected to a circular-velocity component in the plane of M31.

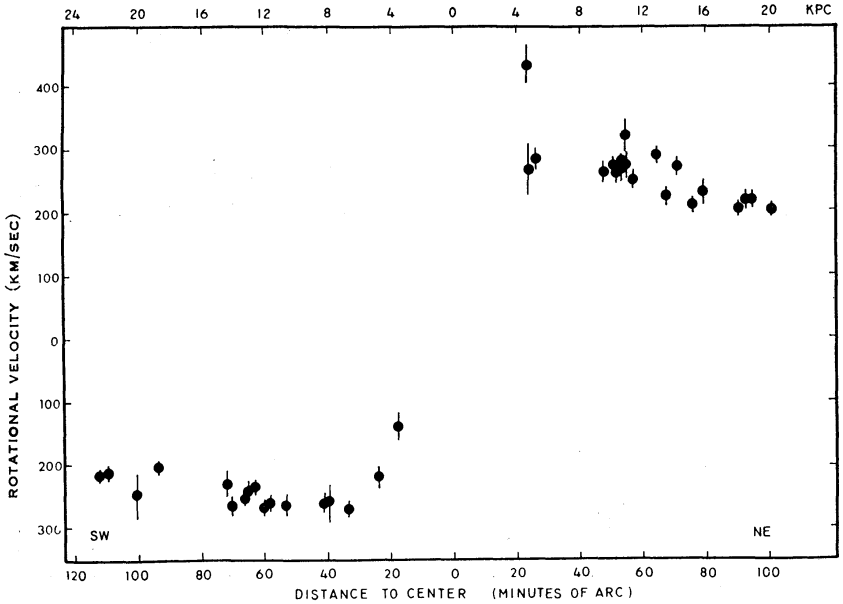

FIG. 4.—Mean rotation velocities for thirty-four OB associations plus three outer regions in M31, as a function of distance from the center. Error bars indicate average error of the velocity of the association, calculated from the velocities of individual emission regions in the association, or from the observational errors, whichever are larger.

If we form a mean rotational velocity for each association, then the scatter in Figure 3 is considerably reduced, as shown in Figure 4. The mean rotational velocity for each of the thirty-four associations is plotted; also included are rotational velocities for three additional regions (Arp 249, 250, 502) with large R, all farther from the nucleus than the van den Bergh associations. The error bars mark either the average external error, calculated from the scatter in the rotational velocities among the association members, or the internal observational error projected as described above, whichever is larger. We shall use the data from Figures 3 and 4 to determine a rotation curve for M31 in § V below.

IV. THE OBSERVED VELOCITIES $R < 16'$ (3.2 KPC)

There are no identified emission regions within 16′ (3.2 kpc) of the nucleus of M31. Hence, it is not possible to study the velocity field of this inner region by the methods employed above. Although absorption lines are present in the spectrum from the inte-

grated starlight of the stellar component near the nucleus, velocity measurements from absorption lines are inherently of much lower accuracy than those from emission lines. One emission feature, the [O II] λ3727 doublet, has been previously observed and measured within 2′ (400 pc) of the nucleus by Babcock (1939) and by Münch (1960, 1962). Our early plates across the nucleus showed a sharp [N II] λ6583 emission line extending out from the nucleus, superimposed on the background continuum. Even though the background continuum is stronger in the red spectral region than in the blue, there is no difficulty in measuring accurate velocities from this sharp emission line.

We have, therefore, taken a series of spectra crossing the inner region of M31. A record of observations is listed in Table 2. For each plate the image of the galaxy was held fixed on the slit. Along the major axis, the plates cover most of the range from SW 233 pc to NE 1800 pc. At the 84-inch telescope, the slit subtends 470 pc in M31 along the major axis; along the minor axis, due to the foreshortening of the galaxy, the slit subtends 2100 pc. Observations extend along the minor axis from SE 4.1 kpc to NW 2.3 kpc. The

TABLE 2

OBSERVATIONS NEAR NUCLEUS OF M31

Plate	Date (U.T.)	Exposure (min.)	Position Angle	Location of Slit*
L1331a	1967 September 9	20	38°	Nucleus centered SW 30″–NE 30″
L1331b	1967 September 9	8	38°	Nucleus centered SW 30″–NE 30″
L1381	1967 October 9	74	39°	NE major axis 105″–195″
KP 1575a	1968 November 18	15	68°	30° to NE major axis 13″–153″
KP 1575b	1968 November 18	24	68°	30° to NE major axis 13″–153″
KP 1578	1968 November 18	169	128°	NW minor axis 13″–153″
KP 1581	1968 November 19	180	128°	SE minor axis 13″–153″
KP 1583	1968 November 19	50	38°	NE major axis 13″–153″
KP 1584	1968 November 19	120	38°	NE major axis 193″–333″
KP 1591	1968 November 20	20	38°	Nucleus centered SW 70″–NE 70″
KP 1592	1968 November 20	210	38°	NE major axis 406″–546″
KP 1593	1968 November 20	229	128°	SE minor axis 137″–277″

NOTE.—L = Lowell; KP = Kitt Peak.

* Along major axis (P.A. = 38°), 60″ = 200 pc. Along minor axis, 60″ = 889 pc.

[N II] λ6583 emission line is seen on all plates; He I λ5876 emission is sometimes present (but difficult to separate from a nearby weak nightsky line); Hα emission is seen only rarely. The [O II] λ3727 emission line is present on all plates, out of focus in second order. No other emission lines are observed. There is every evidence that the [N II] λ6583 emission line could be traced even farther from the nucleus than the range of our observations. Only a lack of observing time prevented more extensive coverage.

In Figure 5 (Plate 3) we reproduce a series of the nuclear spectra; the [N II] line is marked. The intensity of the [N II] line decreases with increasing distance from the nucleus. The [N II] line is no broader than the instrumental profile. For our spectra, this is 5 Å, or 250 km sec^{-1} at 6583 Å. A similar observation concerning each component of the [O II] doublet was made by Münch (1960).

For all plates, velocities have been measured from the [N II] line, as a function of distance from the center. On plates where the emission line is sometimes indistinct, only the sharpest points have been measured. Observed velocities along the major axis, as a function of distance from the nucleus, are shown in Figure 6. No adjustments of any kind have been made to the measured points. Different symbols represent the measures from the seven different plates. To reduce the observed velocities to velocities in the plane of M31, all velocities must be increased by 1.026. The open circles, $R > 15'$ (3.0 kpc) represent the velocities measured for the innermost emission regions.

For two plates (1331b, 1591) emission has been measured at the nucleus, with velocities $V = -297$ km sec^{-1} and $V = -307$ km sec^{-1}; the systemic velocity of M31 has been chosen to agree with these measures. Along the NE major axis, the velocity rises sharply to $R = 400$ pc with a maximum velocity of 225 km sec^{-1} with respect to the nucleus. It then decreases to about 50 km sec^{-1} with respect to the nucleus at $R = 1.6$ kpc. The velocity measured by Münch from the [O II] line extends only to $R = 2'$ (400 pc), but the agreement between the two sets of observations is excellent, as is seen in Figure 7.

It should be pointed out that the observed maximum in the velocities at $R = 400$ pc is not the maximum observed in the nucleus of M31 by Lallemand, Duchesne, and Walker (1960). These authors obtained spectra of the center of M31 at very high dispersion (48 Å mm^{-1}) and observed a maximum in the rotation curve at $R = 2''$ (7 pc). Their

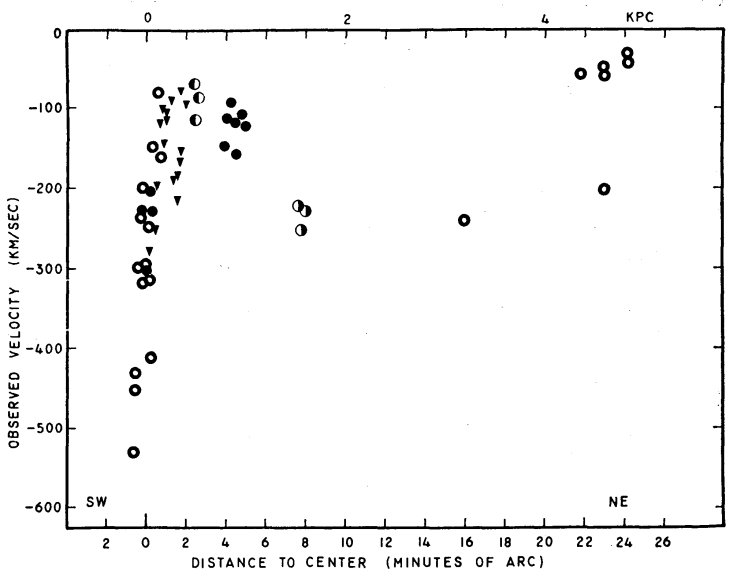

FIG. 6.—Observed velocities along the NE major axis of M31 from the [N II] λ6583 emission line. For $R \leq 8'$, different symbols represent different plates. For $R > 15'$, open circles indicate velocities of innermost emission regions.

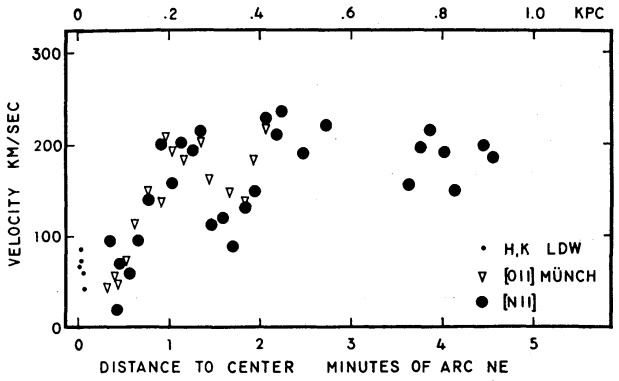

FIG. 7.—Observed velocities along the NE major axis of M31, very near the nucleus, projected to the plane of M31. Emission-line velocities from [O II] λ3727 (Münch 1962) and [N II] λ6583 are shown. Small dots represent the absorption-line velocities from H and K, obtained by Lallemand, Duchesne, and Walker (1960) for $R < 4''$.

velocities are plotted in Figure 7. The scale of our spectrograms perpendicular to the dispersion and the resolution of our image-tube system are not sufficient to observe such an effect. The minima in the rotational velocities at $R = 4''$, $2'$, and $8'$ (13, 400, and 1600 pc) produce a sawtooth appearance for the inner rotation curve.

In order to study the dynamics of the inner region of M31, it is of fundamental importance to know if the motions of the excited gas, as observed in the [O II] and [N II] lines, correspond to the motions of the stellar component near the nucleus, and if the gas we are observing is in equilibrium in the large-scale gravitational field of the galaxy. If this is the case, the observed velocity of the gas is the projection on the line of sight of predominantly circular motions. It would not be the case if the excited gas arose recently from explosive phenomena and was being expelled from the nucleus. In this latter case, the observed velocities are merely the radial-velocity component of three-dimensional noncircular motions. However, we believe that the observed velocities of the gaseous component do correspond to the velocities of the stellar component, for two reasons.

First, we have measured the velocities of the stellar component near the nucleus from the Fe I λ5270 absorption line on our plates. The sodium D-lines are not satisfactory for this purpose, both because they are a doublet of 6 Å separation and because the sodium emission line from the terrestrial night sky shifts its position with respect to the M31 absorption line as the observed velocities in M31 vary from -300 to -100 km sec^{-1} for this region of the nucleus. The prominent MgH blend is also not satisfactory for velocity measurements. The adopted line is fairly narrow and of about equal intensity on all of our plates. It is an unresolved blend (λ5269.541 + λ5270.360) and is in the comparison Fe + Ne spectrum. The comparison line is marked in Figure 5; the absorption line from M31 is seen displaced to the blue. For three plates (1584, 1591, and 1592) the measured velocities from the absorption line are in agreement with the emission-line velocities for the same plates, and exhibit the steep rise and the inner maximum in the rotation curve. The sole exception is plate 1583, for which the absorption-line velocities are several hundred kilometers per second too negative with respect to the emission-line velocities on the same plate. There is no explanation for this single discrepancy, although plate 1583 is darker than the other plates and it may be an exposure effect. We are satisfied that to the accuracy of the absorption-line velocities along the NE major axis there is evidence from our observations that the stellar and gaseous components have the same motions.

Second, the rotation curve near the nucleus of M31 derived by Babcock (1939) from measures of the H- and K-lines and the G-band (all absorption lines) also indicates a steep velocity rise from the origin, to a maximum velocity of about 100 km sec^{-1} at $R =$ 600 pc, followed by a decrease to almost zero velocity at $R = 1.6$ kpc. In position, this maximum and minimum are in agreement with our emission-line observations; in magnitude, the velocity maximum is only about half of that which we observe. However, the poorer velocity resolution (1 μ = 22.6 km sec^{-1} at the K-line on Babcock's plates) plus the greater difficulty in measuring a diffuse absorption line does not make this difference unreconcilable. In addition, although no velocities from the [O II] emission line are published by Babcock, he states that the emission-line velocities agreed satisfactorily with the absorption-line velocities; the range in R is not stated. We are therefore satisfied that the similarities between the absorption-line velocities and the emission-line velocities arise from similar motions of the stellar and gaseous populations near the nucleus of M31, and that we can use the observed velocities of the [N II] line to study the mass in the galaxy.

Along the minor axis of M31, the observed velocities will equal the systemic velocity if only circular motions are present. However, the [N II] λ6583 velocities (Fig. 8) exhibit a series of maxima and minima, with typical velocities of about ± 100 km sec^{-1} over regions of 500 pc in the galaxy. The most notable departure from the systemic velocity is near $R = 1$ kpc on the SE (far) side, where velocities of $+100$ km sec^{-1} with respect

to the central velocity are observed. It was Münch's (1960) observations of similar velocities from the [O II] λ3727 line that led him to infer that gas was streaming from the nucleus of M31. Our observations confirm this, as may be seen from the agreement of the [N II] and the [O II] velocities in Figure 8. The observation that the gas in the region near $R = 2$ kpc has very low circular velocity implies that the gas is expelled from the nucleus with almost zero angular momentum.[2]

There are many unanswered questions concerning the presence of the [N II] emission line near the nucleus of M31. We do not yet know why Hα is only weakly observed, what the mechanism is for exciting the [N II] line, and what causes the decrease in intensity of [N II] with increasing distance from the nucleus. It is known that in some emission regions and planetary nebulae in our Galaxy as well as near the nucleus of many galaxies, the [N II] λ6583 line is stronger than Hα. This effect is observed in the emission regions in M31 also. For all emission regions with $R > 5$ kpc the intensity ratio Hα/[N II] > 1; for all regions with $R < 5$ kpc, Hα/[N II] ≤ 1. It is of interest that Peimbert (1968) has

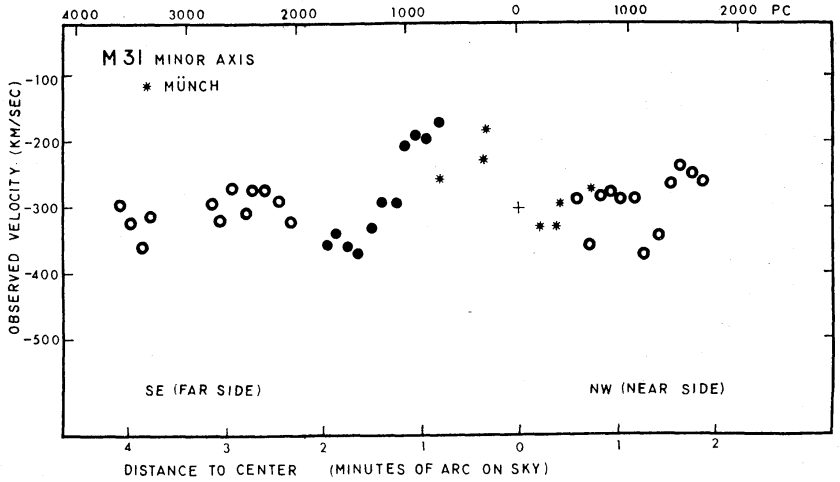

FIG. 8.—Observed velocities along the minor axis of M31, measured from the [N II] λ6583 emission line. Different symbols represent different plates. Cross at $R = 0$, $V = -300$ km sec^{-1} marks the systemic velocity of the galaxy. Stars indicate the velocities measured by Münch (1960) from the [O II] λ3727 emission line.

shown that in the nuclei of M51 and M81 an abundance increase of nitrogen relative to hydrogen near the nucleus is most likely responsible for the increased intensity of [N II] there. The relative line strengths for the emission regions of M31 from our spectra are still being studied.

The mechanism for excitation of the [N II] line depends on the history of the gas. If the excited gas is in dynamical equilibrium, then a small number of early-type stars in the nucleus of the galaxy could supply the excitation energy. Minkowski and Osterbrock (1959) have suggested this mechanism for the production of emission lines in the nuclei of elliptical galaxies. Recent OAO-II satellite observations of the nucleus of M31 in the ultraviolet by Code and Bless (Goldberg 1969) indicate that the radiant energy from the nucleus increases with decreasing wavelength. This phenomenon, too, is consistent with a galaxy in which there are a few early-type stars in the nucleus.

Alternatively, if the gas has been expelled in an explosive event, then the event must have provided the energy for excitation. However, the nucleus of M31 does not contain a radio source, such as Sgr A in our own Galaxy. This is consistent with our belief that the ionized nitrogen is in dynamical equilibrium. We shall therefore assume that the

[2] We are indebted to Professor Oort for pointing this out.

velocities measured for the NE major axis represent rotational velocities near the nucleus.

V. THE ROTATION CURVE AND MASS OF M31

There are a variety of ways in which we can form a rotation curve from the observed velocities. For the region $R < 1.6$ kpc, the [N II] emission-line velocities are used. For the region $R > 1.6$ kpc, various rotation curves have been formed, based on four different groupings of the data, as follows:

1) all observed velocities (Fig. 3),

2) mean velocities for OB associations (Fig. 4),

3) velocities for all regions within $\pm 25°$ of the major axis, plus all inner regions, $R < 7.0$ kpc,

4) velocities for all regions within 1 kpc of the major axis ($|Y| \leq 5'$).

As there are only minor differences between the various rotation curves and resulting masses, they will not be discussed in detail. For all data samples, the rotation curve is symmetrical about $V = -300 \pm 5$ km sec^{-1}, so this value has been adopted as the central velocity.

In the range $1 < R < 3.6$ kpc there is only one observed velocity, the value from the outermost [N II] measurement. Hence, there is considerable uncertainty in the rotation-curve minimum near $R = 2$ kpc. Generally, calculations have been made with a low minimum and a higher minimum, to indicate the range of acceptable solutions. Likewise, the fact that the velocities of the outermost points near $R = 22.6$ kpc are not decreasing with increasing R results in rotation curves from some polynomials which are increasing for large distances. In these cases also, two solutions have generally been made: one which fits the observed points, and another which remains flat near $R = 24$ kpc.

We show in Figure 9 the rotational velocities observed from the [N II] emission across the nucleus, plus the velocities from the OB associations. The solid line $R < 1.6$ kpc is a fifth-order polynomial, if the small dip near $R = 400$ pc is neglected. For $R > 2.6$ kpc, the curve is a fourth-order polynomial least-squares fit required to remain flat near $R = 24$ kpc. Points with $\epsilon \geq 26$ km sec^{-1} (in the rotational velocity) have been given half-weight in the solution. The two curves have been required to join smoothly near $R = 2$ kpc. The dashed curve is a second representation of the minimum, which is arbitrarily drawn as shown. As will be seen below, this higher minimum has the property that the density is everywhere positive, which is not true for the lower minimum.

The dispersion of the velocities about the rotation curve in Figure 9 is small, except for the region near 4 kpc. The average residual velocity from the curve is 18 km sec^{-1} for all points, or 13 km sec^{-1} if the three high velocities near $R = 4$ kpc are neglected. This latter value is of the order of the velocity dispersion within each association and of the observational errors projected to the plane of M31, so the actual dispersion about the rotation curve must be less than this.

Various methods for determining the mass distribution and the total mass of a galaxy from a rotation curve have been extensively described by Perek (1962), so they will not be discussed here. We assume a disk model for M31. Then the relation between circular velocity V and mass out to $a = R$ is given by (Kuzmin 1952; Brandt 1960)

$$M(R) = \frac{2}{G\pi} \int_0^R \frac{V^2(a)\,a\,da}{(R^2 - a^2)^{1/2}}. \tag{3}$$

With the substitution $a = R \sin \theta$, equation (3) is in a form suitable for numerical integration. Integration has been carried out on an IBM 1130. For the two rotation curves shown in Figure 9, the resulting mass distributions are tabulated in Table 3 and plotted in Figure 10. Also included in the table are the mass distributions for a solution with low mass and for one with higher mass. The values for the total mass out to $R =$

24 kpc are 1.66×11^{11} $M_\odot$ (low minimum) and 1.67×11^{11} $M_\odot$ (higher minimum); those for the mass in the nucleus to $R = 1$ kpc are 5.2×10^9 $M_\odot$ and 6.2×10^9 $M_\odot$, respectively. When these values are increased 10 percent to compensate for the assumption of a flat disk (Brandt 1960), the total mass is 1.8×10^{11} $M_\odot$ out to 24 kpc. Also shown in Figure 10 are the variation in the mass surface density as a function of distance from the center, and the variation in the angular velocity, V/R, as a function of R. Note that the solution with the high inner minimum has a positive mass density everywhere. The solution with the low minimum has a negative surface density near $R = 1$ kpc. We take this to mean only that the density at this distance is vanishingly small for the low-minimum model.

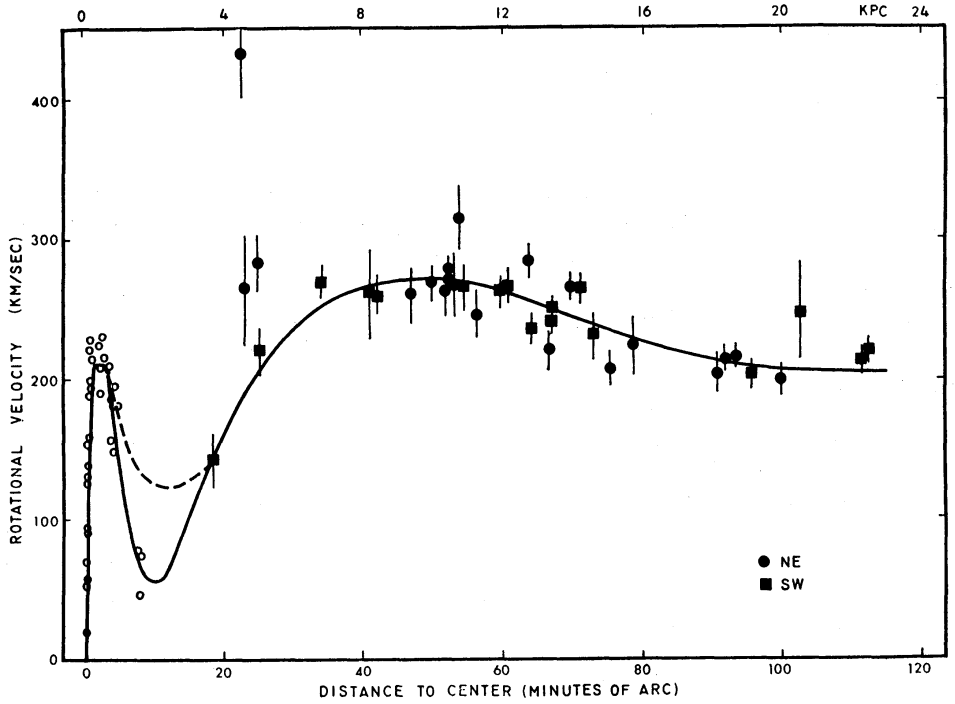

FIG. 9.—Rotational velocities for OB associations in M31, as a function of distance from the center. *Solid curve*, adopted rotation curve based on the velocities shown in Fig. 4. For $R \leq 12'$, curve is fifth-order polynomial; for $R > 12'$, curve is fourth-order polynomial required to remain approximately flat near $R = 120'$. Dashed curve near $R = 10'$ is a second rotation curve with higher inner minimum.

Various other rotation curves for the data in Figures 3 and 4 have been formed, all from least-squares solutions, with polynomials of third, fourth, or sixth order. In Figure 11 we show, superimposed, the fourteen rotation curves from the polynomial representations. The various mass determinations from these rotation curves are listed in Table 4. Successive columns list the order of the polynomial, the resulting total mass, 1.1 times the mass, and the value of the maximum distance to which the mass has been determined. The final columns list the depth of the inner minimum, and notes concerning the solutions.

It is apparent from the calculations that there is only a small spread in total mass out to $R = 24$ kpc from all fourteen solutions. The shaded regions in Figure 12 indicate the range of masses which results from the fourteen rotation curves, as well as the range of surface densities. For the mass out to $R = 24$ kpc, a value of $M = (1.68 \pm 0.1) \times 11^{11}$ $M_\odot$ lies midway between all values. When this is increased 10 percent to compensate for the disk approximation, we obtain a mass $M = (1.85 \pm 0.1) \times 11^{11}$ $M_\odot$ out to $R = 24$ kpc; the error is estimated from the total range in values. For the entire galaxy,

1970ApJ...159..379R

TABLE 3

MASS MODELS FOR M31

	Model 5			Model 6			Model 2			Model 11		
r (kpc)	V (km sec^{-1})	1.1×Mass ($10^{10}M\odot$)	Density ($M\odot$ pc^{-2})	V (km sec^{-1})	1.1×Mass ($10^{10}M\odot$)	Density ($M\odot$ pc^{-2})	V (km sec^{-1})	1.1×Mass ($10^{10}M\odot$)	Density ($M\odot$ pc^{-2})	V (km sec^{-1})	1.1×Mass ($10^{10}M\odot$)	Density ($M\odot$ pc^{-2})
0.....	0	...	...	0	...	...	0	...	...	0	...	...
0.2....	165	0.064	+2560	170	0.068	2730	170	0.069	2730	165	0.064	+2560
0.4....	227	0.274	+4160	231	0.283	4280	231	0.284	4280	227	0.274	+4160
0.6....	228	0.480	+2720	234	0.498	2860	234	0.498	2860	228	0.480	+2720
0.8....	197	0.580	+ 995	212	0.629	1290	212	0.630	1290	197	0.580	+ 995
1.....	154	0.575	− 30	183	0.680	400	183	0.680	400	154	0.575	− 30
2.....	53	0.316	− 108	127	0.710	84	127	0.710	84	53	0.316	− 108
3.....	99	0.416	+ 169	127	0.880	125	127	0.880	125	48	0.266	− 20
4.....	157	1.05	+ 336	157	1.35	272	171	1.51	325	174	0.994	+ 555
5.....	201	2.17	+ 408	201	2.38	390	205	2.56	376	250	2.96	+ 700
6.....	232	3.64	+ 419	232	3.81	409	231	3.91	386	278	5.15	+ 559
7.....	254	5.32	+ 391	254	5.47	386	250	5.47	367	281	7.03	+ 384
8.....	266	7.06	+ 344	266	7.18	340	263	7.12	332	274	8.45	+ 259
9.....	272	8.73	+ 286	272	8.83	285	271	8.77	288	266	9.61	+ 191
10.....	272	10.2	+ 230	272	10.3	228	273	10.3	241	261	10.6	+ 161
11.....	268	11.6	+ 178	268	11.6	177	272	11.7	193	259	11.7	+ 151
12.....	262	12.7	+ 134	262	12.7	133	267	13.0	147	259	12.8	+ 147
13.....	254	13.6	+ 98	254	13.6	97	257	13.9	108	260	13.9	+ 139
14.....	245	14.2	+ 71	245	14.3	71	249	14.7	74	259	15.0	+ 122
15.....	236	14.8	+ 52	236	14.8	51	239	15.2	47	255	16.0	+ 97
16.....	227	15.2	+ 39	227	15.2	38	227	15.5	27	247	16.8	+ 66
17.....	220	15.5	+ 31	220	15.6	31	216	15.7	13	226	17.2	+ 35
18.....	214	15.9	+ 27	214	15.9	27	206	15.8	5	223	17.5	+ 12
19.....	209	16.2	+ 26	209	16.2	26	198	15.9	3	211	17.5	− 2
20.....	206	16.5	+ 28	206	16.5	27	192	15.9	5	200	17.4	− 4
22.....	203	17.3	+ 32	203	17.3	32	190	16.3	25	194	17.6	+ 18
24.....	202	18.3	+ 33	202	18.3	33	206	17.6	65	195	18.4	+ 22

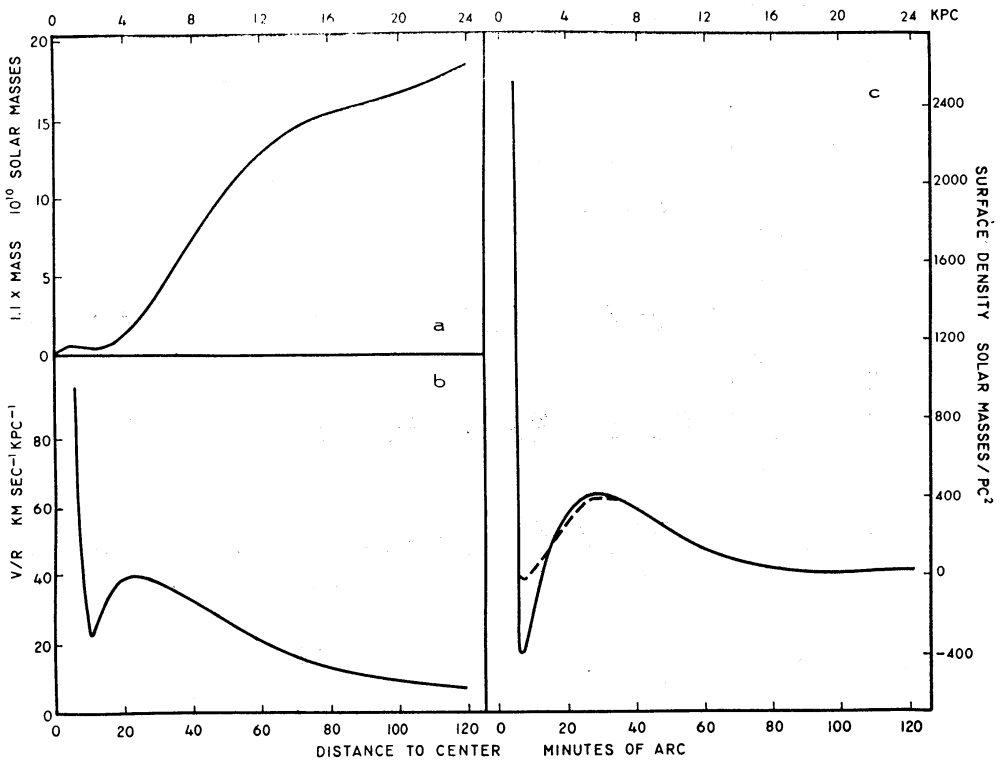

FIG. 10.—(*a*) Total mass of M31 out to $R = 24$ kpc determined from rotation curve (Fig. 9), as a function of distance from the center, and multiplied by 1.1 to compensate for flat disk approximation. (*b*) Angular velocity, V/R, for M31, calculated from rotation curve, as a function of distance from center. (*c*) Surface density for M31, determined from rotation curve, as a function of distance from center. Solid curve and dashed curve are calculated from corresponding curves in Fig. 9.

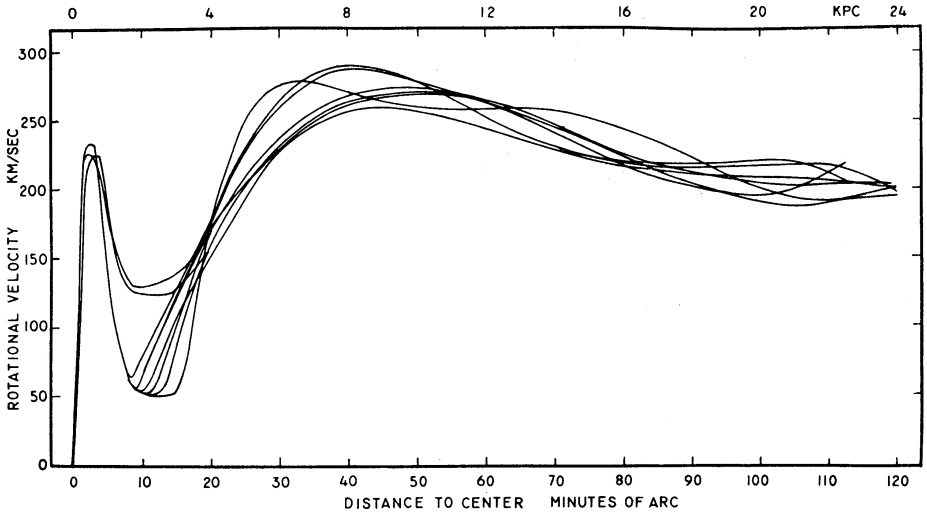

FIG. 11.—Fourteen rotation curves for M31; seven least-squares polynomial representations for $R >$ 13′, each with high and low minimum. Details are contained in Table 4.

the average mass surface density is 100 $M_\odot$ pc^{-2}. There is no significant change in the total mass from small variations in the rotation curve, from a change of adopted inclination of the galaxy, with the depth of the inner minimum, or with the height of the inner maximum. The total mass is sensitive to the slope of the rotation curve for large R.

Because this value of the total mass of M31 appears low in comparison with recent

TABLE 4

MASS DETERMINATIONS FOR M31

Number	Outer Polynomial Order	Mass ($10^{11} M_\odot$)	1.1×Mass ($10^{11} M_\odot$)	Outermost R (kpc)	Inner Minimum	Notes
1	3	1.60	1.76	24	low	1,5
2	3	1.60	1.76	24	high	1,5
3	3	1.65	1.82	22.8	low	1
4	3	1.65	1.82	22.8	high	1
5	4	1.66	1.83	24	low	1,6
6	4	1.66	1.83	24	high	1,6
7	4	1.75	1.93	24	low	1,5
8	4	1.75	1.93	24	high	1,5
9	4	1.71	1.88	22.8	low	1
10	4	1.72	1.89	22.8	high	1
11	6	1.67	1.84	24	low	2,5
12	6	1.68	1.85	24	high	2,5
13	4	1.63	1.79	24	low	3
14	4	1.64	1.80	24	high	3
15	2 concentric disks	1.56	1.72	20	...	4

Notes (solutions 1–14 are solutions of Kuzmin integral; solution 15 is procedure of Wyse and Mayall 1942):
1. OB associations plus three outer regions, $\xi = 77°$.
2. H II regions within 25° of major axis plus those with $R < 35'$, $\xi = 77°$.
3. OB associations plus three regions, $\xi = 74°$.
4. Only fair fit to rotational velocities.
5. Additional point at $R = 24$ kpc to prevent rotation curve from rising.
6. Additional point at $R = 3$ kpc and $R = 24$ kpc.

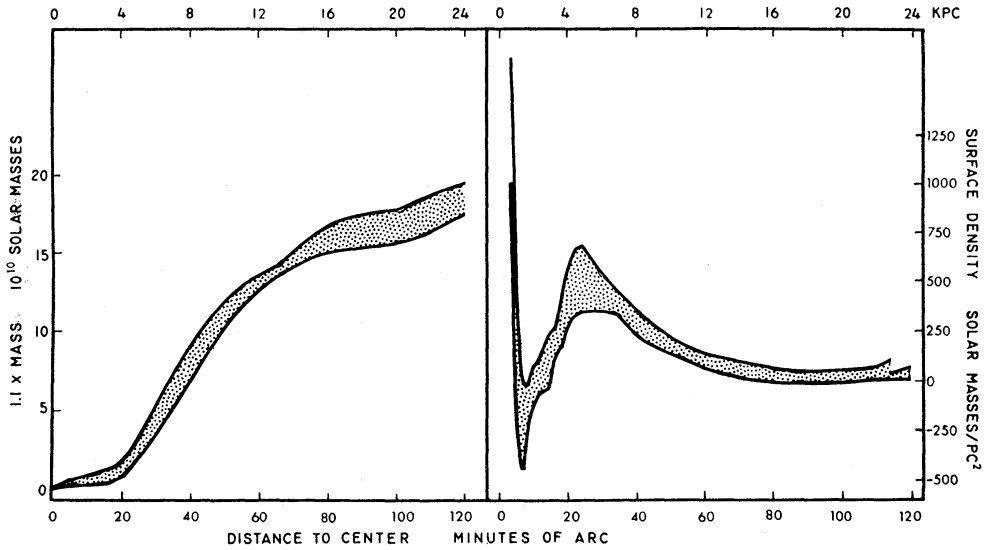

FIG. 12.—*Left:* range of calculated values of total mass for M31, as a function of distance to center, for fourteen rotation curves (Fig. 11). Dotted region indicates range of fourteen multiply intersecting curves. *Right:* range of calculated values of surface density of M31, as a function of distance to center. Dotted region indicates range of multiply intersecting curves.

determinations (Brandt 1960; Roberts 1966), it is necessary to examine the cause of this difference. It has been customary in recent studies to fit the circular velocities with a Brandt rotation curve of the form

$$V_c = \frac{AB}{(1 + B^n R^n)^{3/2n}},$$

where the parameters A, B, and n are determined by the shape of the rotation curve. We prefer not to adopt this approach, because the Brandt curve rises steeply from the origin and is a poor fit to our observations for $R < 6$ kpc. With a rotation curve of the Brandt type, the total mass out to infinity is immediately given, based on the assumption of a law of inverse-square force far from the nucleus. From the calculations of Brandt (1960) for M31 it is seen that, of the total mass $M = 3.7 \times 11^{11}\ M_\odot$, only 57 percent lies within $R = 24$ kpc. Thus, to within the distance of our farthest observed point, the mass from the Brandt solution is $M = 2.1 \times 11^{11}\ M_\odot$, close to the value determined above.

It does not appear possible, from the presently available data, to infer anything about the mass beyond 24 kpc in M31. The mass density near $R = 24$ kpc is extremely sensitive to the shape of the rotation curve in this region, and hence is of low accuracy. We know that the density is low beyond $R = 24$ kpc; the important question is how soon it becomes negligible. No optical emission regions were found by Baade beyond $R = 24$ kpc; no OB associations were found by van den Bergh beyond $R = 18$ kpc. Radio observations have detected 21-cm radiation beyond this distance, but there are two circumstances which complicate the analysis. First, on the north side of M31 the observed velocities are near zero, so the radiation from M31 becomes confused with the local hydrogen near the Sun. On the south end of the galaxy, the southwest companion (Burke, Turner, and Tuve 1964) contributes to the 21-cm radiation. In the model studies of Burke, Turner, and Tuve, a negative hydrogen density was necessary between the disk of M31 and the southwest companion, indicating a vanishingly small density. Eventually, it will be possible to make 21-cm observations of the outer parts of M31 which will establish the amount of neutral hydrogen. For the present, we prefer to adopt as the mass of M31 that mass contained within the outermost observed point; extrapolation beyond that distance is clearly a matter of taste.

Additional solutions, using the procedure adopted by Wyse and Mayall (1942), resulted in a curve which is only a fair approximation to the rotation curve; resulting values for the mass are included in Table 4. An attempt to fit the circular velocities with an algebraic curve of the form suggested by Toomre (1964) did not produce a satisfactory fit.

From the mass distribution determined above, and the variation of luminosity in M31 derived by de Vaucouleurs (1958), we find the mass-luminosity ratios for successive distances from the center shown in Table 5. The mass is the mass within the distance R, from Model 5, Table 3. The estimated uncertainty comes from the range in solutions shown in Figure 12. The luminosity given by de Vaucouleurs is scaled to the adopted distance for M31, and shown in column (4). The ratio M/L is given in column (5). For the entire galaxy a mass-luminosity ratio of about 12 ± 1 appears to be the best value.

VI. COMPARISON OF OPTICAL AND RADIO RESULTS

It is of interest to compare the rotation curve and mass determinations from the optical observations with the results available from 21-cm observations. It is important to reiterate that the radio resolution is still poor by optical standards. For M31, the highest-resolution studies use a 10′ beam (Burke, Turner, and Tuve 1964; Roberts 1966); at the distance of M31 this corresponds to a circle on the sky of 2 kpc radius, and on M31 itself to an ellipse with major and minor axes 2 kpc by 9 kpc due to the foreshortening

of the galaxy. Any details with scale sizes smaller than this must be inferred from the velocity resolution and models of the mass distribution.

The observations of Burke, Turner, and Tuve (1964) were restricted to a band within $\pm 5'$ of the major axis, to a distance $R = 28$ kpc. Figure 13 shows the rotation curve which results if we select from our optical observations (Table 1) only regions with $|Y| \leq 5'$, again using mean values for members of OB associations. The solid curve is the SW rotation curve of Burke, Turner, and Tuve (1964) and is a good fit to both the SW and NE optical velocities. That the asymmetry which they observed is not apparent

TABLE 5

MASS-LUMINOSITY RATIOS FOR M31

R (min. of arc) (1)	R (kpc) (2)	$\int M$ to R ($10^{10} M\odot$) (3)	$\int L$ to R ($10^{10} L\odot$) (4)	$\int M/L$ to R (5)
15.....	3	0.416±0.4*	0.42	1.0±1†
30.....	6	3.64 ±0.8	0.64	5.7±1
45.....	9	8.73 ±0.9	0.83	10 ±1
60.....	12	12.7 ±0.5	0.99	13 ±0.5
90.....	18	15.9 ±1	1.30	12 ±0.8
120.....	24	18.3 ±1	1.37	13 +0.7

* Uncertainty is estimate from range of solutions shown in Fig. 12.

† Uncertainty in M only.

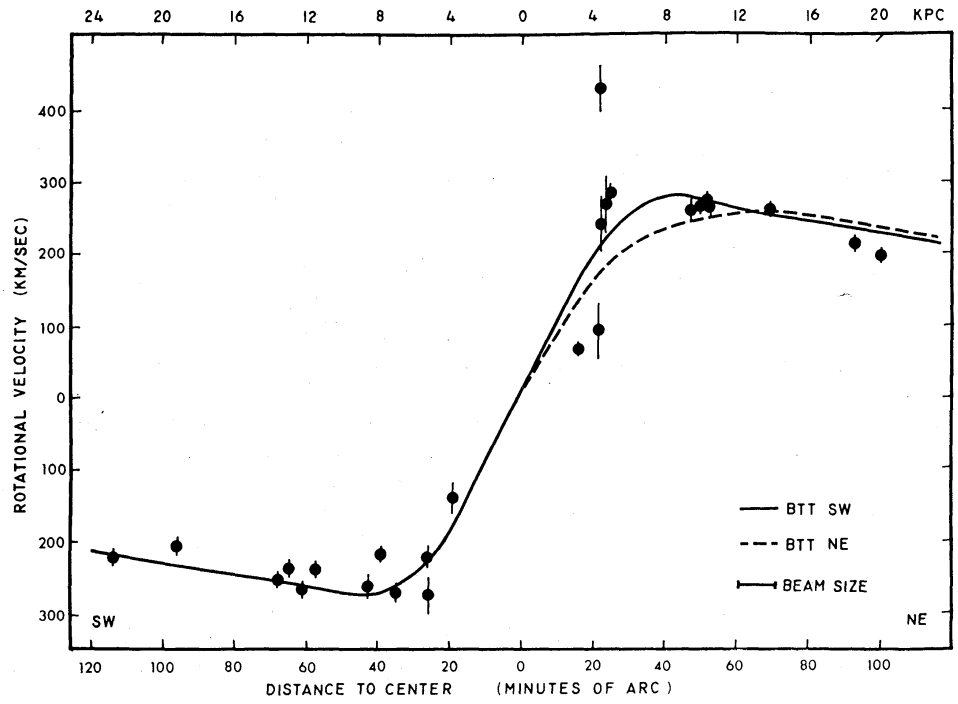

FIG. 13.—Rotational velocities for twenty-five emission regions in M31, within $\pm 5'$ of the major axis, as a function of distance from the center. Error bars indicate average error. *Solid line*, rotation curve of Burke, Turner, and Tuve (1964) from 21-cm H I rotation curve for SW side; *dashed line*, rotation curve for NE side.

in the optical observations may be seen by noting that their southwest curve is a better fit to the northeast optical points than is their northeast curve. The total mass determined from their density model is $M = 2.4 \times 11^{11}\ M_\odot$, only slightly higher than that derived above.

The rotation curve determined by Roberts (1966) is a least-squares fit to circular velocities observed in the NW and SE quadrants of M31, computed from the observed coordinates of the peak signal at a given observed velocity. Observations cover much of the galaxy, but no observations were made for $R > 16$ kpc along the major axis. Circular velocities for points with $R > 16$ kpc come only from points nearer the minor axis, as do many of the points for $R < 16$ kpc. Hence there is no point-to-point coincidence of velocities observed by Roberts and regions observed by us.

The circular velocities have been fitted by Roberts (1966) with a Brandt rotation curve. The curve is very flat, with a maximum of 250 km sec^{-1} at $R = 9$ kpc. This is lower than the maximum observed in the optical velocities. The total mass to infinity determined from the 21-cm observations is $3.1 \times 11^{11}\ M_\odot$, which reduces to $1.8 \times 11^{11}\ M_\odot$ within $R = 24$ kpc.

Gottesman, Reddish, and Davies (1966) have derived a rotation curve from major-axis observations, which is in good agreement with the curve of Roberts. The mass which they derive for M31 is $M = 2.4 \times 11^{11}\ M_\odot$ to $R = 30$ kpc.

There is thus substantial agreement between the optical and 21-cm observations of velocities in M31. The rotation curve from the optical velocities extends to $R = 24$ kpc, which is no less than that of the 21-cm observations. The scatter of the optical velocities is no greater than the scatter in the radio observations. Because there are only negligible differences between the rotation curves from the optical and the 21-cm observations, there is no significant difference in the derived mass for M31.

A lower limit to the total mass of neutral hydrogen is also obtained from the 21-cm observations, and we may compare its distribution with the distribution of total mass in M31. From the surface density derived by Burke, Turner, and Tuve (1964) from model studies, the total H I mass within $R = 24$ kpc is $M \geq 6.1 \times 10^9\ M_\odot$ for an adopted distance of 620 kpc, if symmetry in the plane of M31 is assumed. For a distance of 690 kpc, the revised total H I mass is $M \geq 6.7 \times 10^9\ M_\odot$. This lower limit is larger by a factor of 2 than the H I mass derived by Argyle (1965). It is confirmed by observations of M31 made with the 300-foot Green Bank telescope by Roberts (unpublished) which give a total mass of H I of $5.1 \times 10^9\ M_\odot$, obtained by integrating the velocity profiles over the entire galaxy.

Turner (private communication) has estimated that the actual value of the total H I mass may be a factor of 2 greater than this lower limit, because the assumption of optically thin clouds may not be valid, and because the H I regions in M31 do not fill the telescope beam. Hence, the ratio of the H I mass to the total mass is between 4 and 8 percent to $R = 24$ kpc, or 4–8 times the generally quoted value (Kerr and Westerhout 1965). This increase arises both because of the greater value for the H I content to $R = 24$ kpc and because of the small total mass to $R = 24$ kpc. The ratio of total H I mass to total mass is plotted as a function of R in Figure 14. The error bars mark the uncertainty in this ratio, calculated from (1) the ranges of total mass of M31 derived from the optical observations and (2) the difference in the H I distribution between the north side and the south side of M31 from Burke, Turner, and Tuve (1964). The ratio of the H I density to the mass density at each R is small for $R < 8$ kpc, and is essentially flat at about 7 percent from 14 to 24 kpc. Of the total gravitational mass in M31 out to $R = 24$ kpc, one-half is contained in the disk of radius 9 kpc, but the disk containing one-half of the H I mass has a radius of 13 kpc.

VII. COMPARISON OF M31 WITH OUR GALAXY

The parameters derived for M31 may be compared with those of our Galaxy. There is a built-in bias, however, for many of the dynamical parameters for our Galaxy have

often previously been adopted to make the general features of our Galaxy conform with those of M31. For example, the rotation curve of Rougoor and Oort (1960) has been determined by a comparison of the Galactic system and M31. We first consider the rotation curves; we use the mass model of Schmidt (1965). Because we are interested in the large-scale features of our Galaxy, this model is more suited to a comparison than the detailed rotation curve, $4 < R < 10$ kpc, of Shane and Bieger-Smith (1966). Schmidt points out that circular velocities in our Galaxy are known only for seven values of R, $R \leq 10$ kpc. Beyond $R = 10$ kpc, the rotation curve is an extrapolation, chosen so that the density decreases as R^{-4}. These known values for V_{rot} are plotted in Figure 15, along with the rotation curve adopted by Schmidt (1965). Schmidt did not try to fit the inner maximum, which comes from the observations of Rougoor and Oort (1960). We have also plotted in Figure 15 the rotation curve for M31.

The rotation curve adopted by Schmidt, but modified to include the two innermost points, is rather similar to the rotation curve of M31, although the very deep minimum near $R = 2$ kpc is not shown for our Galaxy. There is evidence, however, that the rota-

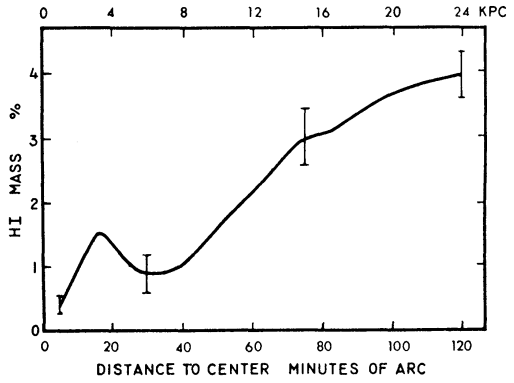

FIG. 14.—Ratio of $M_{H\,I}$, the H I mass out to distance R, to the total mass out to distance R in M31, as a function of distance from the center. H I mass is only a lower limit; see text for details.

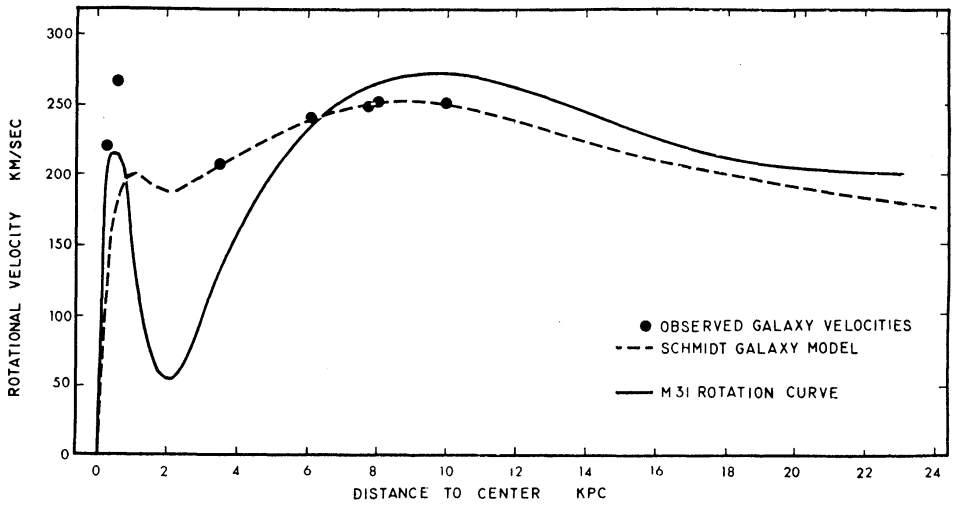

FIG. 15.—Comparison of rotation curves for M31 and the Galaxy, as a function of distance from the center. *Solid line*, rotation curve for M31 (Fig. 9); *dashed line*, rotation curve from Schmidt model of the Galaxy. *Filled circles*, observed rotational velocities for the Galaxy (Rougoor and Oort 1960; Schmidt 1965).

tion velocities in our Galaxy are very small just outside the rapidly rotating nucleus. This evidence comes from the 21-cm observations toward the nucleus. Both Rougoor (1964) and Burke and Tuve (1964) noted that their observations implied very low circular velocities in this region, although the final rotation model adopted by Rougoor (1964) was a compromise, and a less deep minimum was used. Burke and Tuve concluded that either ω or $d\omega$ ($\omega = V/R$) must increase with increasing R, or the arms in our Galaxy must be leading, to agree with the observed 21-cm velocities near $l = 0°$. It is clearly very difficult to infer the structure of the inner parts of our Galaxy if there is an inner minimum in the rotation curve, because V/R will be triple-valued in some directions toward the center, and there will be six values of R along the line of sight from the Sun to beyond the center which will have the same value of V/R. Such a possibility should be kept in mind, however, in the unraveling of the spiral pattern of our Galaxy as contained in the 21-cm observations.

The general model of the disk of our Galaxy which emerges from the 21-cm observations is as follows (Oort 1968; Kerr and Westerhout 1965; Woltjer 1965). The central source is surrounded by a rapidly rotating disk; rotational velocities are about 200 km sec^{-1} at $R = 100$ pc, and are then approximately constant near $V = 250$ km sec^{-1} to $R = 1$ kpc. At $R \sim 1$–3 kpc, the gas density is low, and there is a large systematic radial component in the velocities, decreasing from $V = 200$ km sec^{-1} to $V = 50$ km sec^{-1}. Rotational velocities in this region are sometimes very low. Oort (1968) has suggested as possible causes of the expansion motions the action of asymmetrical gravitational fields in the Galaxy, the pressure of magnetic fields, or eruptive activity near the nucleus, with the last possibility being the least likely. Beyond $R = 4$ kpc, the rotational velocities increase to a maximum $V = 250$ km sec^{-1} near $R = 10$ kpc, and decrease slowly thereafter.

Although there is no source in M31 like the Sgr A source in the center of our Galaxy, the remaining model of the Galaxy described above applies well to M31. There is a rapidly rotating nucleus, with rotational velocities above $V = 200$ km sec^{-1} within a few hundred parsecs of the center. Near $R = 1$ kpc, gas is observed leaving the nucleus with velocities of $V = 100$ km sec^{-1}. At about $R = 2$ kpc, there is a region of vanishingly small mass and rotational velocities which are very low. At the outer edge of this region, near $R = 4$ kpc, the velocity dispersion is high, higher than in any other observed region of M31. Beyond $R = 4$ kpc, the rotational velocities in M31 are about 20 km sec^{-1} higher than those in corresponding regions in our Galaxy, but the shapes of the rotation curves are reasonably similar.

From the rotation curve for the Galaxy, Schmidt determined a total mass of $M = 1.8 \times 11^{11}\ M_\odot$, of which one-half is located interior to the spheroidal surface with axial ratio 0.05 through the Sun. A mass of about $1.5 \times 11^{11}\ M_\odot$ is contained within $R = 24$ kpc. Thus with the current distance scale for M31, M31 is about 20 percent more massive than the Galaxy. The maximum circular velocity for M31 is 270 ± 10 km sec^{-1}, compared with 250 km sec^{-1} for our Galaxy. Hence, merely decreasing the distance of M31 would not improve the coincidence of the two rotation curves, although it would decrease the mass of M31.

At the position of the Sun, the Schmidt model adopts Oort's constants $A = +15$ km sec^{-1} kpc^{-1}, $B = -10$ km sec^{-1} kpc^{-1}, $V/R = 25$ km sec^{-1} kpc^{-1}. The resulting mass surface density is 145 $M_\odot$ pc^{-2}, and the logarithmic density gradient $r(d \log \rho/dr) = -1.8$. For the mass model adopted for M31, A increases from $A = 5.9$ at $R = 6$ kpc to $A_{max} = 14.7$ at $R = 11.6$ kpc and decreases thereafter; B increases from $B = -32.9$ at $R = 6$ kpc to $B = -5.4$ at $R = 13$ kpc. The values $A = 14.6$, $B = -10.3$ at $r = 10.8$ kpc are most similar to those at the position of the Sun. Here, $V/R = 25$ km sec^{-1} kpc^{-1}, and the logarithmic density gradient is -1.2. However, the mass surface density is $180 \pm 30\ M_\odot$ pc^{-2}, which is higher than the Schmidt value at the Sun. It must be pointed out, however, that the Schmidt value is very sensitive to the density adopted in the

regions $R > 10$ kpc. For M31, the total mass interior to $R = 10.8$ kpc is $1.1 \times 10^{11} M_\odot$.

For our Galaxy, the ratio of H I mass to total mass is between 4 and 7 percent (Kerr and Westerhout 1965; Westerhout 1968); for M31, as determined above, it is between 4 and 8 percent.

Finally, we can examine the velocity dispersion of H II regions in the Galaxy. Miller's (1968) recent study of galactic H II regions indicates that the majority of H II regions in the vicinity of the Sun have velocities that are well represented by a mean rotation curve. For emission regions in the Orion and the Sagittarius arms, the velocity dispersion in the radial velocities is significantly less than 10 km sec^{-1}. For the Perseus arm, however, systematic deviations from the mean rotation curve are present, both for the 21-cm and for the optical velocities. In M31, the average dispersion in the rotational component about the rotation curve is 13 km sec^{-1}, if the three high points near $R = 4$ kpc are neglected. There is thus no significant difference in velocity dispersion between H II regions in the Galaxy and those in M31.

VIII. NONCIRCULAR MOTIONS IN M31

In the preceding analysis, the assumption has been made that only circular motions are present in M31, so that the term in equation (1) containing $E(R)$ is zero. In order to test the validity of this assumption, a series of solutions has been made with $E(R) \neq 0$. For all emission regions in a single arm, the distance from the nucleus, R, is approximately constant. Hence, equation (1) can be solved for V and E, assumed constant for a small interval in R. Solutions have been made with $V_c = -300$ km sec^{-1}, and $\xi = 77°$ and $\xi = 74°$. We show in Table 6 the values of V and E obtained in the solution with $\xi = 77°$; there is no significant difference with $\xi = 74°$.

TABLE 6

NONCIRCULAR MOTIONS IN M31

Arm	Number of H II Regions	Range in R	Range in θ	$\langle V \rangle_{E=0}$ (km sec^{-1})	$\langle V \rangle$ (km sec^{-1})	$\langle E \rangle$* (km sec^{-1})
3.....	9	22′.1– 25′.5	48°–293°	262±29	260±31	+ 0.1±14
4.....	19	47′.4– 56′.2	8°–330°	259± 7	258± 6	−14 ± 6
5.....	12	64′.3– 75′.7	32°–359°	235±10	246± 8	+30 ±10
6+7.....	12	79′.4–120′.1	7°–346°	222± 8	223± 8	− 9 ±12
6+7.....	8	93′.4–120′.1	7°–346°	226±13	223±14	−16 ±24

* $\langle E \rangle$ = mean expansion velocity at $\langle R \rangle$.

With the exception of arms 4 and 5, no evidence for noncircular motions is present. For these arms, expansion velocities just 3 times the mean error are found. However, an investigation of the individual velocities in each arm reveals that there is no extended region in M31 over which only positive or only negative expansion motions are present. Instead, there are a few regions with large deviations from circular motions which may be better fitted by equation (1) with $E \neq 0$, but the remaining regions, even for a small angular extent in the galaxy, have deviations from the mean circular velocity which imply both positive and negative values for E. Even for the region of large dispersion in velocities near $R = 4$ kpc, no simple model of systematic motions radial from the center of M31 will reduce the scatter. From this we conclude that a few emission regions in M31 exhibit velocities which are significantly different from the mean circular velocity. However, for the majority of H II regions, the velocity dispersion is no larger than the uncertainty in the circular velocities, and there is no correlation between position in the galaxy and scatter about the mean circular velocity. There is no evidence for systematic noncircular motions larger than 15 km sec^{-1}, outside the nuclear regions.

IX. CONCLUSIONS

Spectra of 67 H II regions from 3 to 24 kpc from the nucleus of M31 have been obtained with the DTM image-tube spectrograph at a dispersion of 135Å mm^{-1}. Radial velocities, principally from Hα emission, have been determined with an accuracy of 10 km sec^{-1} for most regions. Rotational velocities have been calculated under the assumption of circular motions.

For the region interior to 3 kpc where no H II regions have been identified, spectra reveal the [N II] λ6583 emission line superimposed on the continuum from the integrated starlight of the nucleus of M31. Velocity measures for the emission line indicate a rapid rotation in the nucleus, rising to a maximum circular velocity of $V = 225$ km sec^{-1} at $R = 400$ pc, and falling to a deep minimum near $R = 2$ kpc.

From the rotation curve for $R \leq 24$ kpc, the following disk mass model of M31 results. There is a dense, rapidly rotating nucleus of total mass $M = (6 \pm 1) \times 10^9\ M_\odot$. Near $R = 2$ kpc the density is very low and the rotational velocities are very small. In the region from 500 pc to 1.4 kpc (most notably on the SE side), ionized gas is observed moving out from the nucleus with a velocity which decreases with increasing distance from the center, and with almost zero angular momentum.

Beyond $R = 4$ kpc the total mass of the galaxy increases approximately linearly to about $R = 14$ kpc, and more slowly thereafter. The total mass to $R = 24$ kpc is $(1.85 \pm 0.1) \times 11^{11}\ M_\odot$; one-half of this mass is located in the disk interior to $R = 9$ kpc. In contrast, a lower limit to the H I mass determined from 21-cm observations is $6.7 \times 10^9\ M_\odot$; half of it is contained in the disk interior to $R = 13$ kpc. The ratio of H I to total mass in M31 is thus between 4 and 8 percent.

Within a single emission region, the average error of the velocity in the radial component is less than 10 km sec^{-1}; for several regions within a single OB association the average deviation from the mean radial velocity is less than 10 km sec^{-1}; the average deviation about the mean rotation curve is less than 15 km sec^{-1}. All of these are close to the observational uncertainty. No evidence for noncircular motions is found.

The rotation curve from the optical observations for $R \geq 3$ kpc agrees moderately well with the rotation curve from the 21-cm observations. The maximum rotational velocity, $V = 270 \pm 10$ km sec^{-1}, is slightly higher than that obtained from 21-cm observations.

There is a similarity between the M31 rotation curve and that adopted by Schmidt (1965) for our Galaxy, especially if the rotation curve for our Galaxy is modified to include the inner maximum observed by Rougoor and Oort (1960). However, the rotation curve for M31 has a slightly higher maximum and decreases more slowly with large R, resulting in a 20 percent larger mass for M31 than for our Galaxy.

We would like to thank Dr. J. S. Hall, Director of the Lowell Observatory, and Dr. N. U. Mayall, Director of the Kitt Peak National Observatory, for making telescope time available, and Dr. G. E. Kron for kindly making available copies of Baade's marked charts. We wish to thank Drs. S. D'Odorico, M. S. Roberts, R. J. Rubin, K. C. Turner and M. A. Tuve for valuable conversations, and S. van den Bergh for supplying the photograph of M31.

APPENDIX

TABLE A1

RECORD OF OBSERVATIONS

Emission Region (Arp)	Plate	Date (U.T.)	Exposure (min)	Velocity (km sec^{-1})	Weight
23	1374	1967 October 8	67	−219	1
24	1374	1967 October 8	67	−228	1
55	1373	1967 October 8	60	−248	1
55	1516	1968 September 21	60	−235	0.75
74	1377	1967 October 9	60	−123	1
75	1377	1967 October 9	60	−116	1
95	1372	1967 October 8	60	−176	0.5
97	1372	1967 October 8	60	−176	1
97	1515	1968 September 21	60	−199	1
162	1376	1967 October 9	108	−146	1
162a	1376	1967 October 9	108	−148	1
165	1376	1967 October 9	108	−143	1
167	1376	1967 October 9	108	− 97	1
184	1370	1967 October 8	60	−115	1
184	1567	1968 October 26	90	−158	1
185	1370	1967 October 8	60	− 69	0.5
185	1567	1968 October 26	90	−144	0.5
204	1355	1967 October 6	58	− 38	1
204	1568	1968 October 26	92	− 51	1
204a	1355	1967 October 6	58	− 37	1
210	1321	1967 September 7	50	− 23	0.75
210	1523	1968 September 22	50	− 52	1
212	1321	1967 September 7	50	− 55	0.5
212	1523	1968 September 22	50	− 37	0.5
216	1320	1967 September 7	53	− 65	1
216	1522	1968 September 22	50	− 94	0.75
217	1320	1967 September 7	53	− 59	0.5
236	1521	1968 September 22	89	−135	1
236	1540	1968 October 22	80	−124	1
249	1509	1968 September 20	62	− 89	1
249	1510	1968 September 20	59	− 95	1
250	1343KP	1967 October 2	75	−109	0.75
250	1526	1968 October 19	74	−126	0.5
250	1553	1968 October 24	82	−108	1
275	1534	1968 October 21	70	−423	1
275	1549	1968 October 24	85	−457	0.5
284	1328	1967 September 9	60	−389	1
284	1490	1968 September 17	90	−397	1
289	1182	1966 December 15	57	−516	0.5
289	1327	1967 September 9	40	−521	1
290	1191	1966 December 17	60	−406	0.5
290	1394a	1967 October 11	62	−380	1
297	1329	1967 September 9	59	−447	1
297	1394b	1967 October 11	60	−451	1
297	1491	1968 September 17	85	−467	1
303	1503	1968 September 19	120	−490	0.75
303	1541	1968 October 22	80	−522	1
312	1495	1968 September 18	77	−565	1
312	1496	1968 September 18	78	−569	1
320	1183	1966 December 15	60	−462	0.5
320	1393a	1967 October 11	60	−507	1
330	1330	1967 September 9	50	−498	0.5
330	1500	1968 September 19	63	−500	0.5
338	1489	1968 September 17	66	−533	0.75
338	1544	1968 October 23	100	−529	1
343	1498	1968 September 19	30	−561	0.75
343	1499	1968 September 19	58	−533	0.75
352	1481	1968 September 15	75	−493	1
359	1349KP	1967 October 4	55	−539	1
359	1482	1968 September 15	70	−553	1

TABLE A1—*Continued*

Emission Region (Arp)	Plate	Date (U.T.)	Exposure (min)	Velocity (km sec^{-1})	Weight
360	1349KP	1967 October 4	55	−510	1
360	1482	1968 September 15	70	−535	1
379	1346KP	1967 October 3	15	−527	1
379	1483	1968 September 15	45	−560	1
380	1387	1967 October 10	60	−488	1
380	1566	1968 October 26	87	−461	1
415	1551	1968 October 24	90	−389	1
415a	1551	1968 October 24	90	−436	0.5
416	1550	1968 October 24	93	−461	1
423	1338	1967 September 11	65	−453	1
423	1365	1967 October 7	50	−439	1
429	1366	1967 October 7	45	−431	1
464	1179	1966 December 14	120	−589	0.5
464	3193b	1967 October 11	66	−506	1
464	1494	1968 September 18	70	−554	0.75
478	1350KP	1967 October 4	57	−503	1
478	1488	1968 September 17	70	−505	1
478	1545	1968 October 13	90	−511	1
479	1350KP	1967 October 4	57	−483	1
479	1545	1968 October 23	90	−479	1
484	1351KP	1967 October 4	62	−513	1
484	1484a	1968 September 15	70	−528	1
484	1484b	1968 September 15	50	−539	0.75
493	1547	1968 October 23	89	−444	1
493	1552	1968 October 24	79	−474	1
494	1547	1968 October 23	89	−505	1
494	1552	1968 October 24	79	−515	1
500	1385	1967 October 10	59	−523	1
500	1560	1968 October 25	85	−473	1
502	1352KP	1967 October 4	56	−519	1
502	1490	1968 September 7	90	−509	1
519	1375	1967 October 8	56	−157	1
519	1558	1968 October 25	90	−156	1
521	1519b	1968 September 21	56	−264	1
521a	1519b	1968 September 21	56	−208	1
565	1360a	1967 October 6	58	−184	1
565	1360b	1967 October 6	41	−142	1
577	1359	1967 October 6	58	−129	1
595	1357b	1967 October 6	75	−188	1
595	1358	1967 October 6	60	−164	1
595	1539	1968 October 22	70	−211	1
599	1369	1967 October 8	60	− 59	0.5
600	1369	1967 October 8	60	− 90	1
616	1357a	1967 October 6	73	− 46	1
616	1538	1968 October 22	73	− 78	1
628	1323	1967 September 7	34	−123	1
628	1524	1968 September 22	57	−148	0.75
666	1309	1967 September 4	60	− 72	1
666	1345KP	1967 October 2	43	− 43	1
666	1525	1968 September 22	24	− 32	1
671	1309	1967 September 4	60	− 57	1
671	1345KP	1967 October 2	43	− 19	1
671	1525	1968 September 22	24	− 27	1
683	1315	1967 September 5	64	−154	0.75
683	1344KP	1967 October 2	60	−133	1
683	1506	1968 September 20	60	−119	1
685	1341KP	1967 October 2	46	−113	0.75
685	1507	1968 September 20	60	−118	1
686	1340KP	1967 October 2	60	−107	1
686	1508	1968 September 20	60	− 84	1
688	1378	1967 October 9	110	− 25	1
688	1527	1968 October 19	135	− 29	0.75
688	1557	1968 October 25	120	− 83	1

TABLE A2

COEFFICIENTS OF POLYNOMIALS OF ROTATION CURVES

	Model 5	Model 6	Model 2	Model 11
Inner polynomial:				
R^6	...	-0.6574×10^{-3}	-0.6574×10^{-3}	...
R^5	+0.01089	+0.04228	+0.04228	+0.01089
R^4	−0.5272	−1.075	−1.075	−0.5272
R^3	+9.480	+14.63	+14.63	+9.480
R^2	−75.47	−87.30	−87.30	−75.47
R	+230.0	+242.6	+242.6	+230.0
Constant	+1.256	+1.783	+1.783	+1.256
Outer polynomial:				
R^6	...	...	...	-0.1944×10^{-7}
R^5	...	...	...	$+0.8869\times10^{-5}$
R^4	-0.1007×10^{-3}	-0.1007×10^{-3}	...	−0.001612
R^3	+0.003728	+0.003728	$+0.9648\times10^{-3}$	+0.1488
R^2	−0.4878	−0.4878	−0.2270	−7.324
R	+25.47	+25.47	+15.53	+181.2
Constant	−185.2	−185.2	−56.46	−1479.

REFERENCES

Argyle, E. 1965, *Ap. J.*, **141**, 750.
Baade, W., and Arp, H. C. 1964, *Ap. J.*, **139**, 1027.
Baade, W., and Mayall, N. U. 1951, in *Problems of Cosmical Aerodynamics* (Dayton, Ohio: Central Air Documents Office), p. 165.
Babcock, H. W. 1939, *Lick Obs. Bull.*, No. 498, p. 41.
Bergh, S. van den. 1964, *Ap. J. Suppl.*, **9**, 65 (No. 86).
Brandt, J. C. 1960, *Ap. J.*, **131**, 293.
Burke, B. F., Turner, K. C., and Tuve, M. A. 1964, *Carnegie Yrb.*, Vol. **63**, p. 341.
Burke, B. F., and Tuve, M. A. 1964, in *The Galaxy and the Magellanic Clouds*, ed. F. J. Kerr and A. W. Rodgers (Canberra: Australian Academy of Science), p. 183.
Deharveng, J. M., and Pellet, A. 1969, *Astr. and Ap.*, **1**, 208.
Goldberg, L. 1969, *Sci. Am.*, **220**, 101.
Gottesman, S. T., Reddish, V. C. and Davies, R. D. 1966, *M.N.R.A.S.*, **133**, 359.
Kerr, F. J., and Westerhout, G. 1965, in *Galactic Structure*, ed. A. Blaauw and M. Schmidt (Chicago: University of Chicago Press) p. 199.
Kuzmin, G. G. 1952, *Pub. Astr. Obs. Tartu*, **32**, 211.
Lallemand, A., Duchesne, M., and Walker, M. F. 1960, *Pub. A.S.P.*, **72**, 76.
Mayall, N. U. 1951, in *The Structure of the Galaxy* (Ann Arbor: University of Michigan Press), p. 19.
Miller, J. S. 1968, *Ap. J.*, **151**, 373.
Minkowski, R., and Osterbrock, D. 1959, *Ap. J.*, **129**, 583.
Münch, G. 1960, *Ap. J.*, **131**, 250.
———. 1962, in *Problems of Extra-Galactic Research*, ed. G. C. McVittie (New York: Macmillan Co.), p. 119.
Oort, J. H. 1968, in *Galaxies and the Universe*, ed. L. Woltjer (New York and London: Columbia University Press), p. 1.
Pease, F. G. 1918, *Proc. Nat. Acad. Sci.*, **4**, 21.
Peimbert, M. 1968, *Ap. J.*, **154**, 33.
Perek, L. 1962, in *Adv. Astr. and Ap.*, **1**, 165.
Roberts, M. S. 1966, *Ap. J.*, **144**, 639.
Rougoor, G. W. 1964, *B.A.N.*, **17**, 381.
Rougoor, G. W., and Oort, J. H. 1960, *Proc. Nat. Acad. Sci*, **46**, 1.
Rubin, V. C., and D'Odorico, S. 1969, *Astr. and Ap.*, **2**, 484.
Schmidt, M. 1965, in *Galactic Structure*, ed. A. Blaauw and M. Schmidt (Chicago: University of Chicago Press), p. 513.
Shane, W. W., and Bieger-Smith, G. P. 1966, *B.A.N.*, **18**, 263.
Slipher, V. M. 1914, *Lowell Obs. Bull.*, No. 52.
Toomre, A. 1964, *Ap. J.*, **139**, 1217.
Vaucouleurs, G. de. 1958, *Ap. J.*, **128**, 465.
Westerhout, G. 1968, in *Interstellar Ionized Hydrogen*, ed. Y. Terzian (New York and Amsterdam: W. A. Benjamin, Inc.), p. 638.
Woltjer, L. 1965, in *Galactic Structure*, ed. A. Blaauw and M. Schmidt (Chicago: University of Chicago Press), p. 531.
Wyse, A. B., and Mayall, N. U. 1942, *Ap. J.*, **95**, 24.

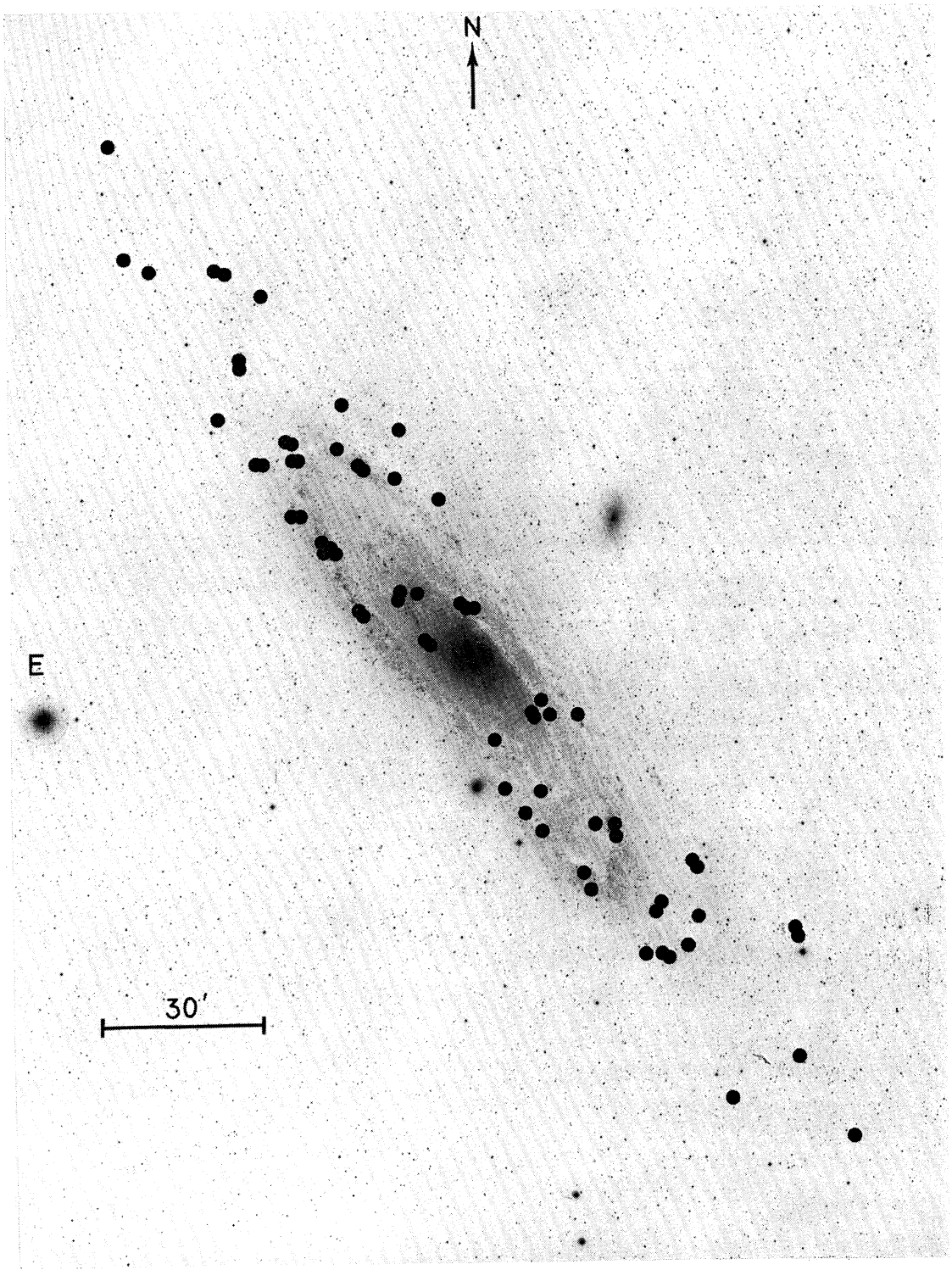

FIG. 1.—Identification chart for emission regions in M31 for which velocities have been obtained. Palomar 48-inch Schmidt ultraviolet photograph, 103aO plate + UG 1 filter, courtesy of Dr. S. van den Bergh.

PLATE 2

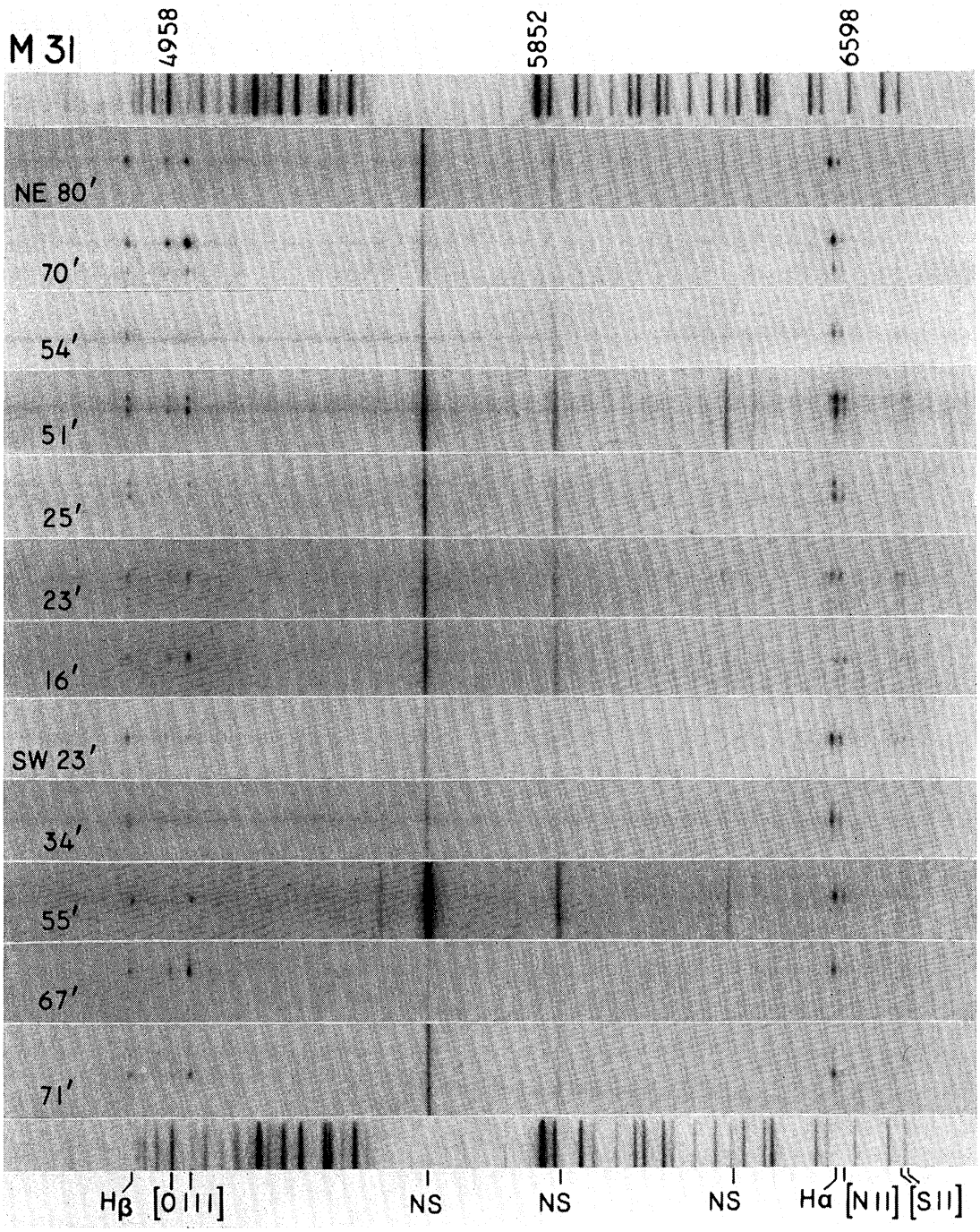

FIG. 2.—Representative spectra of emission regions in M31, arranged according to distance from center. Lines crossing the spectra are nightsky lines. Comparison spectrum is Ne + Fe, original dispersion 135 Å mm^{-1} = 6 km sec^{-1} μ^{-1} at Hα. Principal emission lines are indicated.

RUBIN AND FORD (*see* page 381)

1970ApJ...159..379R

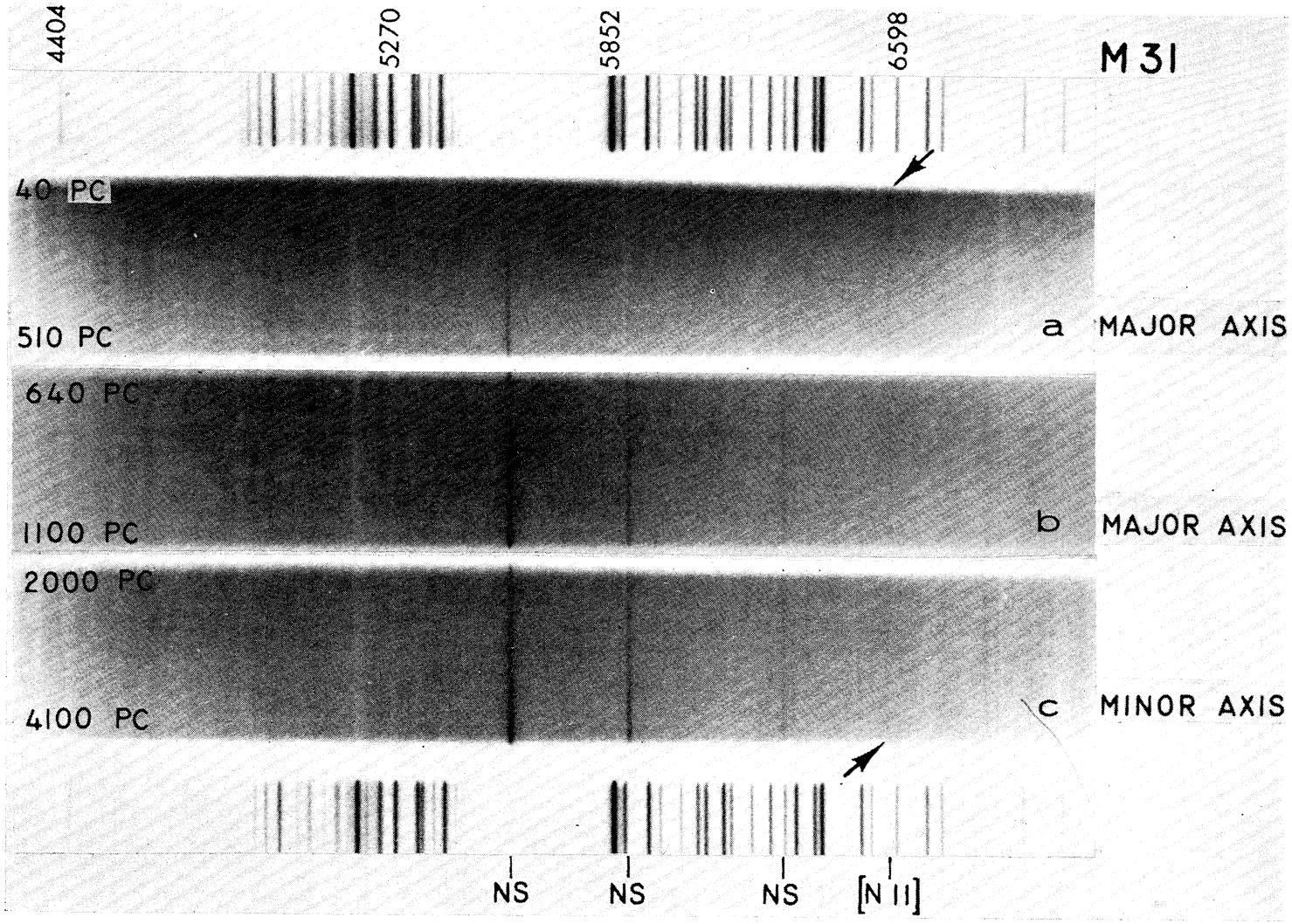

PLATE 3

FIG. 5.—Spectra near the nucleus of M31. (*a*) Plate 1583, NE major axis, 40–510 pc, exposure time 50 min. (*b*) Plate 1584, NE major axis, 640–1100 pc, exposure time 120 min. (*c*) Plate 1593, SE minor axis, 2000–4100 pc, exposure time 229 min. Arrows indicate the [N II] λ6583 emission line.